A physically based distributed karst hydrological model (QMG model-V1.0) for flood simulations

Ji Li[1,*], Daoxian Yuan[1,2], Fuxi Zhang[3], Jiao Liu[4], Mingguo Ma[1]

[1]Chongqing Jinfo Mountain Karst Ecosystem National Observation and Research Station, Chongqing Key Laboratory of Karst Environment, School of Geographical Sciences, Southwest University, Chongqing 400715, China

[2]Key Laboratory of Karst Dynamics, MNR & Guangxi, Institute of Karst Geology, Chinese Academy of Geological Sciences, Guilin 541004, China

[3]College of Engineering Science and Technology, Shanghai Ocean University; Shanghai Engineering Research Center of Marine Renewable Energy 201306, China

[4]Chongqing municipal hydrological monitoring station, Chongqing 401120, China

Corresponding author: Ji Li (445776649@qq.com)

Abstract Karst trough and valleys landforms are prone to flooding, primarily because of the unique hydrogeological features of karst landform, which are conducive to the spread of rapid runoff. Hydrological models that represent the complicated hydrological processes in karst regions are effective for predicting karst flooding, but their application has been hampered by their complex model structures and associated parameter set, especially so for distributed hydrological models, which require large amounts of hydrogeological data. Distributed hydrological models for predicting the Karst flooding is highly dependent on distributed structrues modeling, complicated boundary parameters setting, and tremendous hydrogeological data processing that is both time and computational power consuming. Proposed here is a distributed physically-based karst hydrological model, known as the

QMG (Qingmuguan) model. The structural design of this model is relatively simple, and it is generally divided into surface and underground double-layered structures. The parameters that represent the structural functions of each layer have clear physical meanings, and the parameters are less than those of the current distributed models. This allows modeling in karst areas with only a small amount of necessary hydrogeological data. 18 flood processes across the karst underground river in the Qingmuguan karst trough valley are simulated by the QMG model, and the simulated values agree well with observations, for which the average value of Nash–Sutcliffe coefficient was 0.92. A sensitivity analysis shows that the infiltration coefficient, permeability coefficient, and rock porosity are the parameters that require the most attention in model calibration and optimization. The improved predictability of karst flooding by the proposed QMG model promotes a better mechanistic depicting of runoff generation and confluence in karst trough valleys.

Keywords: Simulation and forecasting of karst floods; Karst trough valleys; QMG (Qingmuguan) model; Parametric optimization; Parameter sensitivity analysis

1 Introduction

Karst trough and valley landformsKarst trough valleys are very common in China, especially in the southwest. In general, these karst areas are water scarce during most of the year because their surfaces store very little rainfall, but they are also potential birthplaces for floods because trough and valley landforms and topographic features facilitate the formation and propagation of floods (White, 2002; Li et al., 2021). The coexistence of drought and flood is a typical phenomenon in these karst trough and valley areas. Taking the example of the present study area, i.e. the Qingmuguan karst trough valley, floods used to happen here constantly during the rainy season. In recent years, with more extreme rainfall events and the increased area of construction land in the region, rainfall infiltration has

decreased and rapid runoff over impervious surfaces has increased, resulting in frequent catastrophic flooding in the basin (Liu et al., 2009). Excess water overflows from karst sinkholes and underground river outlets often occur during floods (Jourde et al., 2007, 2014; Martinotti et al., 2017), flooding large areas of farmland and residential areas and causing serious economic losses (Gutierrez, 2010; Parise, 2010; Yu et al., 2020). Therefore, it is both important and urgent to simulate and predict karst flooding events in karst trough and valleys such as the study area.

Hydrological models can be effective for forecasting floods and evaluating water resources in karst areas (Bonacci et al., 2006; Ford and Williams, 2007; Williams, 2008, 2009). However, modelling floods in karst regions is extremely difficult because of the complex hydrogeological structure. Karst water-bearing systems consist of multiple media under the influence of complex karst development dynamics (Worthington et al., 2000; Kovács and Perrochet, 2008; Gutierrez, 2010), such as karst caves, conduits, fissures and pores, and are usually highly spatially heterogeneous (Chang and Liu, 2015; TeixeiraparenteMario et al., 2019). In addition, the intricate surface hydrogeological conditions and the hydrodynamic conditions inside the karst water-bearing medium result in significant temporal and spatial differences in the hydrological processes in karst areas (Geyer et al., 2008; Bittner et al., 2020).

In early studies of flood forecasting in karst regions, simplified lumped hydrological models were commonly used to describe the rainfall–discharge relationship (e.g. Kovács and Sauter, 2007; Fleury et al., 2007b; Jukić and Denić, 2009; Hartmann et al., 2014a). With the development of physical exploration technology and the progress made in mathematics, computing and other interdisciplinary disciplines, the level of modelling has gradually improved (Hartmann and Baker, 2017; Hartmann, 2018; Petrie et al., 2021), and distributed hydrological models have subsequently become widely used in karst areas. The main difference between lumped and distributed hydrological models is that the latter divide the entire basin into many sub-basins to calculate the runoff generation and confluence, thereby better describing the physical properties of the hydrological processes inside the karst water-bearing system (Jourde et al., 2007; Hartmann, 2018; Epting et al., 2018).

Because of their simple structure and little demand for modelling data, lumped hydrological models have been used widely in karst areas (Kurtulus and Razack, 2007; Ladouche et al., 2014). In a lumped model, the river basin is considered as a whole to calculate the runoff generation and confluence, and there is no division running into sub-basins (Dewandel et al., 2003; Bittner et al., 2020). Lumped models usually consider the inputs and outputs of the model (Liedl and Sauter, 2003; Hartmann and Bake, 2013, 2017). In addition, most of the model parameters are not optimized in a lumped model, and the physical meaning of each parameter is unclear (Chen, 2009; Bittner et al., 2020).

Distributed hydrological models are of active interest in flood simulation and forecasting research (Ambroise et al., 1996; Beven and Binley, 2006; Zhu and Li, 2014). Compared with a lumped model, a distributed model has a more definite physical significance for the model structure in terms of its mechanism (Meng and Wang, 2010; Epting et al., 2018). In a distributed hydrological model, an entire karst basin can be divided into many sub-basins (Birk et al., 2005) using high-resolution digital elevation map (DEM) data. In the rainfall-runoff algorithm of the model, the hydrogeological conditions and karst aquifer characteristics can be considered fully to simulate precisely the runoff generation and confluence (Martinotti et al.,2017; Gang et al., 2019). The commonly used basin distributed hydrological models (i.e. not a special groundwater numerical model such as MODFLOW) have also been applied widely in karst areas and include the SHE/MIKE SHE model (Abbott et al., 1986a,b; Doummar et al., 2012), SWMM model (Peterson and Wicks, 2006; Blansett and Hamlett, 2010; Blansett, 2011), TOPMODEL (Ambroise et al., 1996; Suo et al., 2007; Lu et al., 2013; Pan, 2014) and SWAT model (Peterson and Hamlett, 1998; Ren, 2006).

The commonly used distributed hydrological models have multiple structures and numerous parameters (Lu et al., 2013; Pan, 2014), which means that a distributed model may need vast amounts of data to build its framework in karst regions. For example, the distributed groundwater model MODFLOW-CFPM1 requires detailed data regarding the distribution of karst conduits in a study area (Reimann et al., 2009). Another example is the Karst–Liuxihe model (Li et al., 2019), which has there are fifteen parameters and five

105 underground vertical ~~structures~~layers in the model~~. structure and has 15 parameters, thereby~~

106 Such a complex structure makes the modeling data demand is large, and the modeling in

107 karst area is extremely difficult.~~making it difficult to model in karst areas.~~ In addition, a

108 special borehole pumping test may be required to obtain the rock permeability coefficient.

To overcome the difficulty of the large modelling-data demands for distributed hydrological models in karst areas, a new physically based distributed hydrological model—known as the QMG (Qingmuguan) model-V1.0—was developed in the present study. Other commonly used karst groundwater models with complex structure and parameters—such as the aforementioned MODFLOW-CFPM1 model—require a lot of hydrogeological data for modelling in karst areas (Qin and Jiang, 2014). The new QMG model has a high potential for application in karst hydrological simulation and forecasting. It has certain advantages in its framework and structural design, having a double-layer structure and fewer parameters. The horizontal structure is divided into river channel units and slope units, and the vertical structure below the surface is divided into a shallow karst aquifer and a deep karst aquifer system. This relatively simple model structure reduces the demand for modelling data in karst areas, and only a small amount of hydrogeological data is needed for modelling.

~~To ensure that the QMG model work well in karst flood simulation and prediction in the~~

~~case of relatively simple structure and parameters. We carefully designed the algorithms of~~

~~runoff generation and confluence in the model.~~ To ensure that the QMG model works well in karst flood simulation and prediction despite its relatively simple structure and parameters, we carefully designed the algorithms for runoff generation and confluence in the model. Also, to verify the applicability of the QMG model to flood simulation in karst basins, we selected the Qingmuguan karst trough valley in Chongqing, China as the study area for a flood simulation and uncertainty analysis. In particular, we analysed the sensitivity of the model parameters.

2 Study area and data

2.1 Landform and topography

The Qingmuguan karst trough valley is located in the southeastern part of the Sichuan Basin, China at the junction of the Beibei and Shapingba districts in Chongqing, with the coordinates of 29°40′N–29°47′N, 106°17′E–106°20′E. The basin covers an area of 13.4 km^2 and is part of the southern extension of the anticline at Wintang Gorge in the Jinyun Mountains, with the anticlinal axis of Qingmuguan located in a parallel valley in eastern Sichuan (Yang et al., 2008). The surface of the anticline is heavily fragmented, and faults are extremely well developed with large areas of Triassic carbonate rocks exposed. Under the long-term erosion of karst water, a typical karst trough landforms pattern of 'three mountains and two troughs' has formed (Liu et al., 2009). This karst trough landform provides convenient conditions for flood propagation, and the development of karst landforms is extremely common in the karst region of southwest China, especially in the karst region of Chongqing. Similar regions include the karst trough valley of the Zhongliang Mountains and the Laolongdong karst basin in Nanshan, Chongqing.

The basin is oriented north-north-east and south-south-west in a narrow band of slightly curved arcs and is ~12 km long from north to south. The direction of the mountains in the region is basically the same as that of the tectonic line. The direction of the mountains in the region is generally consistent with the direction of the tectonic line. The difference in relative elevation is 200–300 m. The map in Figure 1 gives an overview of the Qingmuguan karst basin.

Figure 1. The Qingmuguan karst basin.

2.2 Hydrogeological conditions

The Qingmuguan basin is located within the subtropical humid monsoon climate zone, with an average temperature of 16.5 ℃ and an average precipitation of 1250 mm that is concentrated mainly in May–September. An underground river system has developed in the

157 karst trough valley, with a length of 7.4 km, and the water supply of the underground river is

158 mainly rainfall recharge (Zhang, 2012). Most of the precipitation is collected along the hill

159 slope into the karst depressions at the bottom of the trough valley, where it is recharged to

160 the underground river through the dispersed infiltration of surface karst fissures and

161 ~~concentrated injection from~~ sinkholes (Fig. 1a). An upstream surface river collects in a

162 gentle valley and enters the underground river through the Yankou sinkhole (elevation

163 524 m). Surface water in the middle and lower reaches of the river system enters the

164 underground river system mainly through ~~catenuliform~~ cover collapse sinkholes (Gutierrez

165 et al., 2014) or fissures.

166 The stratigraphic and lithologic characteristics of the basin are dominated largely by

167 carbonate rocks of the Lower Triassic Jialingjiang Group (T_{1j}) and Middle Triassic Leikou

168 Slope Group (T_{2l}) on both sides of the slope, with some quartz sandstone and mudstone

169 outcrops of the Upper Triassic Xujiahe Group (T_{3xj}) (Zhang, 2012). The topography of the

170 basin presents a general anticline (Fig. 1b), where carbonate rocks on the surface are

171 corroded and fragmented, high permeability~~with a large permeability coefficient~~. Compared

172 with the core of the anticline, the shale ~~rocks~~ of ~~the two wings of~~ the anticline are less

173 eroded and form a good waterproof layer.

174 To investigate the distribution of karst conduits in the underground river system, we

175 conducted a tracer test in the study area. The tracer was placed into the Yankou sinkhole and

176 recovered in the Jiangjia spring (Fig. 1a,c). According to the tracer test results (Gou et al.,

177 2010), the karst water-bearing medium in the aquifer was anisotropic, ~~whereas the soluble~~

178 ~~carbonate rocks were extremely permeable.~~ and ~~The~~ the karst conduits in the underground

179 river were extremely well developed, and there was a large single-channel underground river

180 about five meters wide. The response of the underground river to rainfall was very fast, with

181 the peak flow observed at the outlet of Jiangjia spring 6–8 h after rainfall based on the tracer

182 test results. The flood peak rose quickly and the duration of the peak flow was short. The

183 underground river system in the study area is dominated by large karst conduits, which is not

184 conducive to water storage in water-bearing media, but is very conducive to the propagation

185 of floods.

2.3 Data

To build the QMG model to simulate the karst flood events, the necessary modelling baseline data had to be collected, including: 1) high-resolution DEM data and hydrogeological data (e.g., the thickness of the epikarst zone, rainfall infiltration coefficient on different karst landforms, and permeability coefficient of rock); 2) land-use and soil type data; and 3) rainfall data in the basin and water flow data of the underground river. The DEM data was downloaded from a free database on the public Internet, with an initial spatial resolution of 30×30 m. The spatial resolution of landuse and soil types were 1000×1000 m, and they were also downloaded from the Internet. After considering the applicability of modelling and computational strength, as well as the size of the basin in the study area (13.4 km^2), the spatial resolution of the three types of data was resampled uniformly in the QMG model and downscaled to 15×15 m based on a spatial discrete method by Berry et. (2010).

The hydrogeological data necessary for modelling was obtained in three simple ways. 1) A basin survey was conducted to obtain the thickness of the epikarst zone, which was achieved by observing the rock formations on hillsides following cutting for road construction. Information was collected regarding the location, general shape, and size of karst depressions and sinkholes, which had a significant impact on compiling the DEM data and determining the convergence process of surface runoff. And the sinkholes in the basin are cover collapse sinkholes (Gutierrez et al., 2014) according to the basin survey. There are 3 large sinkholes (more than 3 meters in diameter) and 12 small sinkholes less than 1 meter in diameter. The rest of the sinkholes between 1 and 3 meters in diameter are 5 in total. The confluence calculation of these sinkholes in the model was based on the results of previous study (Meng et al., 2009). 2) Empirical equations developed for similar basins were used to obtain the rainfall infiltration coefficient for different karst landforms and the permeability coefficient of rock. For example, the rock permeability coefficient was calculated based on an empirical equation from a pumping test in a coal mine in the study area (Li et al., 2019). 3) A tracer experiment was conducted in the study area (Gou et al., 2010) to obtain information on the underground river direction and flow velocity, for

instance, underground karst conduits are well developed in the area, which form an underground river about five meters wide. There is no hydraulic connection between the underground river system in the area and the adjacent basin, means there is no overflow recharge.

Rainfall and flood data are important model inputs, and represent the driving factors that allow hydrological models to operate. In the study area, rainfall data was acquired by two rain gauges located in the basin (Fig. 1a). Point rainfall was then spatially interpolated into basin-level rainfall (for such a small basin area rainfall results obtained from two rain gauges was considered representative). There were 18 karst flood events in the period of 14 April 2017 to 10 June 2019. We built a rectangular open channel at the underground river outlet and set up a river gauge on it (Fig. 1a) to record the water level and flow data every 15 minutes.

3 Methodology

3.1 Hydrological model framework and algorithms

The hydrological model developed in this study was named the QMG model after the basin for which it was developed and to which it was first applied, i.e. the Qingmuguan basin. The QMG model ~~proposed in this study~~ has a two-layer structure, including a surface part and an underground part~~,~~. ~~with the~~The ~~former~~ surface structure mainly performing the calculation of runoff generation and the confluence of the surface river, while the underground structure ~~latter~~ performs the confluence calculation of the underground river system.

The structure of the QMG model is divided into a two-layer structure, both horizontally and vertically. The horizontal structure of the model is divided into river channel units and slope units. The vertical structure below the surface is divided into a shallow karst aquifer (including soil layers, karst fissures and conduit systems in the epikarst zone) and a deep karst aquifer system (bedrock~~rock stratum~~ and underground river system). This relatively simple model structure means that only a small amount of hydrogeological data is needed ~~when modelling~~ in karst regions. Figure 2 shows a flowchart of the modelling and calculation procedures required for the QMG model.

Figure 2. Modelling flow chart of QMG (Qingmuguan) model.

To describe accurately the runoff generation and confluence on a grid scale, these karst sub-basins are further divided into many karst hydrological response units (KHRUs) based on the high-resolution (15 × 15 m) DEM data in the model. The specific steps involved in the division were adopted by referring to studies of hydrological response units (HRUs) in TOPMODEL by Pan (2014). As the smallest basin computing units, the KHRUs can effectively ignore the spatial differences of karst development within the units and reduce the uncertainty in the classification of model units. Figure 3 shows the spatial structure of the KHRUs.

Figure 3. Spatial structure of karst hydrological response units (KHRUs) (Li et al., 2021).

The right-hand side of Figure. 3 shows a three-dimensional spatial model of KHRUs established in the laboratory to reflect visually the storage and movement of water in the karst water-bearing medium with each spatial anisotropy, and to provide technical support for establishing the hydrological model.

The modelling and operation of the QMG model consists of three main stages: 1) spatial interpolation, and the retention of rainfall and evaporation calculations; 2) runoff generation and confluence calculation for the surface river; and 3) confluence calculation for the underground runoff, including the confluence in the shallow karst aquifer and the underground river system.

3.1.1 Rainfall and evaporation calculation

In the QMG model, the spatial interpolation of rainfall is accomplished by a kriging method using the ArcGIS 10.2 software. The Tyson polygon method may be a simpler method for rainfall interpolation if the number of rainfall gauges in the basin is sufficient. The point rainfall observed by the two rainfall gauges in the basin (Fig. 1a) was interpolated spatially into areal rainfall for the entire basin.

Basin evapotranspiration in the KHRUs was mainly vegetal, soil evaporation and water surface evaporation. They were calculated using the following equations (modified from Li et al., 2020):

$$
270 \quad
\begin{cases}
E_v = V^{t+\Delta t} - V^t - P_v \\
E_s = \lambda E_p, \text{if } F = F_c \\
E_s = \lambda E_p \dfrac{F}{F_c}, \text{if } F < F_{sat} \\
E_w = \Delta e \cdot \left[1.12 + 0.62(\Delta T)^{0.9}\right] \cdot \left[0.084 + 0.24\left(1-\gamma^2\right)^{1/2}\right] \cdot \left[0.348 + 0.5\omega^{1.8-1.137\omega^{0.05}}\right]
\end{cases}
\quad (1)
$$

271 Here, E_v [mm] is the vegetal discharge, $V^{t+\Delta t} - V^t$ [mm] is the rainfall variation by

272 vegetation interception, P_v [mm] is the vegetation interception of rainfall and E_s [mm]

273 is the actual soil evaporation. The term λ is the evaporation coefficient. The term E_p

274 [mm] is the evaporation capability, which can be measured experimentally or estimated

275 by the water surface evaporation equation E_w. The term F [mm] is the actual soil

276 moisture, F_{sat} [mm] is the saturation moisture content, F_c [mm] is the field capacity, E_w

277 [mm/d] is the evaporation of the water surface and $\Delta e = e_0 - e_{150}$ [hPa] is the draught

278 head between the saturation vapour pressure of the water surface and the air vapour

279 pressure 150 m above the water surface ~~(150 m above the water surface was selected~~

280 ~~here because the altitude for temperature and humidity observations in the southwestern~~

281 ~~karst regions of China is usually set at 150–200 m)~~. The term $\Delta T = t_0 - T_{150}$ [℃] is the

282 temperature difference between the water surface and the temperature 150 m above the

283 water surface, γ is the relative humidity 150 m above the water surface and ω [m/s]

284 is the wind speed 150 m above the water surface.

285 **3.1.2 Runoff generation**

286 In the QMG model, the surface runoff generation in river channel units means the rainfall in

287 the river system after deducting evaporation losses. This portion of the runoff will

288 participate in the confluence process directly through the river system, rather than

289 undergoing infiltration. In contrast, the process of runoff generation in slope units is more

290 complex, and its classification is related to the developmental characteristics of surface karst

291 in the basin, rainfall intensity and soil moisture. For example, when the soil moisture content

292 is already saturated, there is the potential for excess infiltration surface runoff in exposed

293 karst slope units. The surface runoff generation of the KHRUs in the river channel units and

294   slope units can be described by the following equations (modified from Chen, 2009, 2018;

295   Li et al., 2020):

296
$$
\begin{cases}
P_r(t) = \left[P_i(t) - E_p \right] \dfrac{L \cdot W_{\max}}{A} \\
R_{si} = (P_i - f_i), P_i \geq f_{\max} \\
R_{si} = 0, P_i < f_{\max} \\
f_{\max} = \alpha (F_c - F)^{\beta} + F_s
\end{cases}
\tag{2}
$$

297   Here, $P_r(t)$ [mm] is the net rainfall (deducting evaporation losses) in the river channel units

298   at time t [h], $P_i(t)$ [mm] is the rainfall in the river channel units, L [m] is the length of the

299   river channel, $W_{\max}$ [m] is the maximum width of the river channel selected and A [m^2] is

300   the cross-sectional area of the river channel. R_{si} [mm] is termed the excess infiltration runoff

301   in the QMG model, when the vadose zone is short of water and has not been filled. The

302   infiltration capacity $f_{\max}$ is different in different karst landform units, α, β are the parameters

303   of the Holtan model and F_s [mm] is the stable depth of soil water infiltration.

304   In the KHRUs (Fig. 3), underground runoff is generated primarily from the infiltration

305   of rainwater and direct confluence recharge from sinkholes or skylights. In the QMG model,

306   the underground runoff is calculated by the following equations (modified from Chen,

307   2018):

308
$$
\begin{cases}
R_g = R_0 \exp(-pt^m) \\
R_e = v_e \cdot I_w \cdot z
\end{cases}
\tag{3}
$$

309   where

310
$$
\begin{cases}
\dfrac{\partial R_e}{\partial x} + I_w \cdot z \cdot \dfrac{\partial F}{\partial t} = R_r - R_{epi} \\
v_e = K \cdot \tan(\alpha), \quad F > F_c \\
v_e = 0, \quad F \leq F_c
\end{cases}
\tag{4}
$$

311   Here, R_g [mm] is the underground runoff depth (this part of the underground runoff is mainly

312   from the direct confluence supply of the karst sinkholes or karst windowsskylights in the

313   study area), R_0 [mm] is the average depth of the underground runoff, p and m are attenuation

314   coefficients calculated by conducting a tracer test in the study area, R_e [L/s] is the

315   underground runoff generated from rainfall infiltration in the epikarst zone, I_w [mm] is the

316   width of the underground runoff on the KHRUs, z [mm] is the thickness of the epikarst zone,

317   R_r [mm^2/s] is the runoff recharge on the KHRUs during period t, R_{epi} [mm^2/s] is the water

318   infiltration from rainfall, v_e [mm/s] is the flow velocity of the underground runoff, K

319   [mm/s] is the current permeability coefficient and α is the hydraulic gradient of the

320   underground runoff. If the current soil moisture is less than the field capacity, i.e. $F \leq F_{\text{c}}$,

321   then the vadose zone is not yet full, there will be no underground runoff generation, and

322   rainfall infiltration at this time will continue to compensate for the lack of water in the

323   vadose zone until it is full and before runoff is generated.

324   **3.1.3 Channel routing and confluence**

325   In the QMG model, the calculation of runoff confluence on the KHRUs includes the

326   confluence of surface river channel and underground runoff. There are already many mature

327   and classical algorithms available for calculating the runoff confluence in river channel units

328   and slope units, such as the Saint-Venant equations and Muskingum convergence model. In

329   this study, the Saint-Venant equations were adopted to describe the confluence in the surface

330   river and hill slope units, for which a wave movement equation was adopted to calculate

331   confluence in slope units (Chen, 2009):

332
$$\begin{cases} \dfrac{\partial Q}{\partial x} + L\dfrac{\partial h}{\partial t} = q \\ S_f - S_0 = 0 \end{cases} \tag{5}$$

333   where

334
$$Q = vhL = \frac{L}{n}h^{\frac{5}{3}}S_0^{\frac{1}{2}}. \tag{6}$$

335   Here, we customized two variables a and b:

336
$$\begin{cases} a = (\dfrac{n}{L}S_0^{-\frac{1}{2}})^{\frac{3}{5}} \\ b = \dfrac{3}{5} \end{cases} \tag{7}$$

337   Equation (7) was substituted into Eq. (5) and discretized by a finite-difference method,

338 giving

339

$$
\begin{cases}
\dfrac{\partial Q}{\partial x} + abQ^{(b-1)}\dfrac{\partial Q}{\partial t} - q = 0 \\[2mm]
\dfrac{\Delta t}{\Delta x}Q_{i+1}^{t+1} + a(Q_{i+1}^{t+1})^{b} = \dfrac{\Delta t}{\Delta x}Q_{i}^{t+1} + a(Q_{i+1}^{t})^{b} + q_{i+1}^{t+1}\Delta t
\end{cases}
\tag{8}
$$

340 The Newton–Raphson method was used for the iterative calculation using Eq. (8):

341

$$
\left[Q_{i+1}^{t+1}\right]^{k+1} = \left[Q_{i+1}^{t+1}\right]^{k} - \frac{\dfrac{\Delta t}{\Delta x}\left[Q_{i+1}^{t+1}\right]^{k} + a(\left[Q_{i+1}^{t+1}\right]^{k})^{b} - \dfrac{\Delta t}{\Delta x}Q_{i}^{t+1} - a(Q_{i+1}^{t})^{b} - q_{i+1}^{t+1}\Delta t}{\dfrac{\Delta t}{\Delta x} + ab(\left[Q_{i+1}^{t+1}\right]^{k})^{b-1}}, \tag{9}
$$

342 where Q [L/s] is the confluence of water flow in slope units, L [dm] is its runoff width, h

343 [dm] is the runoff depth and q [dm^2/s] is the lateral inflow on the KHRUs. Here, the friction

344 slope S_f equals the hill slope S_0, and the inertia term and the pressure term in the motion

345 equation of the Saint-Venant equations were ignored. The term v [dm/s] is the flow velocity

346 of surface runoff in the slope units as calculated by the Manning equation, n is the roughness

347 coefficient of the slope units, Q_i^{t+1} [L/s] is the slope inflow in the KHRU at time $t+1$ and

348 Q_{i+1}^{t+1} [L/s] is the slope discharge in the upper adjacent KHRU at time $t+1$.

349   Similarly, the surface river channel confluence was described based on the

350 Saint-Venant equation, where a diffusion wave movement equation was adopted, meaning

351 that the inertia term in the motion equation was ignored:

352

$$
\begin{cases}
\dfrac{\partial Q}{\partial x} + \dfrac{\partial A}{\partial t} = q \\[2mm]
S_f = S_0 - \dfrac{\partial h}{\partial x}
\end{cases}
\tag{10}
$$

353 A finite-difference method and the Newton–Raphson method were used for the iterative

354 calculation of the above equation:

355

$$\left\{ \begin{array}{l} \left[Q_{i+1}^{t+1}\right]^{k+1} = \left[Q_{i+1}^{t+1}\right]^{k} - \dfrac{\dfrac{\Delta t}{\Delta x}\left[Q_{i+1}^{t+1}\right]^{k} + c(\left[Q_{i+1}^{t+1}\right]^{k})^{b} - \dfrac{\Delta t}{\Delta x}Q_{i}^{t+1} - c(Q_{i+1}^{t})^{b} - q_{i+1}^{t+1}\Delta t}{\dfrac{\Delta t}{\Delta x} + cb(\left[Q_{i+1}^{t+1}\right]^{k})^{b-1}} \\[4mm] c = (\dfrac{1}{3600}n\chi^{\frac{2}{3}}S_{f}^{-\frac{1}{2}})^{\frac{3}{5}} \end{array} \right. \qquad (11)$$

356 where Q [L/s] is the water flow in surface river channel units, A [dm^2] is the discharge

357 section area, c is a custom intermediate variable and χ [dm] is the wetted perimeter of the

358 discharge section area.

359   The underground runoff in the model includes the confluence of the epikarst zone and

360 underground river. In the epikarst zone, the karst water-bearing media are highly

361 heterogeneous (Williams, 2008). For example, the anisotropic~~crisscrossed~~ karst fissure

362 systems and conduit systems consist of ~~large~~ the corrosion fractures. When rainfall

363 infiltrates into the epikarst zone, water moves slowly through the small (less than 10cm in

364 this study) karst fissure systems, while it flows rapidly in larger (more than 10cm) conduits.

365 The key to determining the confluence velocity lies in the width of karst fractures. In the

366 KHRUs (Fig. 3), the 10-cm width of the fracture was used as a threshold value (Atkinson,

367 1977) based on the borehole pumping test in the basin, meaning that if the fracture width

368 exceeded 10 cm, then the water movement into it was defined as rapid flow; otherwise, it

369 was defined as slow flow. The confluence in the epikarst zone was calculated by the

370 following equation (modified from Beven and Binley, 2006):

371
$$Q(t)_{ijk} = b_{ijk} \cdot \frac{\Delta h}{\Delta l} R_i C_j \cdot T(t)_{\text{slow/rapid}} \qquad (12)$$

372 where

373
$$\left\{ \begin{array}{l} T(t)_{\text{slow}} = nr\,\dfrac{\rho g R_i C_j L_k}{12v} \\[4mm] T(t)_{\text{rapid}} = \dfrac{K_{ij}\left(e^{-f_{ij}h_{ij}} - e^{-f_{ij}z_{ij}}\right)}{f_{ij}} \end{array} \right. \qquad (13)$$

374 Here, $Q(t)_{ijk}$ [L/s] is the flow confluence in the epikarst zone at time t, b_{ijk} [dm] is the

375 runoff width, $\dfrac{\Delta h}{\Delta l}$ is the dimensionless hydraulic gradient, $T(t)_{\text{slow/rapid}}$ is the

376 dimensionless hydraulic conductivity, ρ [g/L] is the density of the water flow, g [m/s^2] is

377 gravitational acceleration, n is the valid computational units, $R_i C_j L_k$ [L] is the volume of

378 the ijk-th KHRU, v is the kinematic viscosity coefficient, f_{ij} is the attenuation coefficient in

379 the epikarst zone, h_{ij} [dm] is the depth of shallow groundwater and z_{ij} [dm] is the thickness

380 of the epikarst zone.

381   The distinction between rapid and slow flows in the epikarst zone is not absolute. The

382 10-cm width of a karst fracture as the dividing threshold is underrepresented due to the only

383 five limited boreholes have been tested for pumping in the region.also has some subjectivity.

384 In fact, there is usually water exchange between the rapid and slow flows at the junction of

385 large and small fissures in karst aquifers. In the QMG model, this water exchange can be

386 described with this equation (modified form Li et al., 2021):

387
$$\begin{cases} Q = \alpha_{i,j,k}\left(h_n - h_{i,j,k}\right) \\ \alpha_{i,j,k} = \sum_{ip=1}^{np} \dfrac{\left(K_w\right)_{i,j,k}\, \pi d_{ip}\, \dfrac{1}{2}\left(\Delta l_{ip}\tau_{ip}\right)}{r_{ip}} \end{cases} \qquad (14)$$

388 Here, $\alpha_{i,j,k}$ [dm^2/s] is the water exchange coefficient in the ijk-th KHRU, $\left(h_n - h_{i,j,k}\right)$

389 [dm] is the water head difference between the rapid and slow flows at the junction of large

390 and small fissures in KHRUs, np is the number of fissure systems connected to the adjacent

391 conduit systems, $\left(K_w\right)_{i,j,k}$ [dm/s] is the permeability coefficient at the junction of a fissure

392 and conduit, d_{ip} and r_{ip} [dm] are the conduit diameter and radius, respectively, Δl_{ip}

393 [dm] is the length of the connection between conduits i and p, and τ_{ip} is the conduit

394 curvature. Some of the parameters in this equation, such as $\left(K_w\right)_{i,j,k}$ and $\left(h_n - h_{i,j,k}\right)$,

395 were obtained by conducting an infiltration test in the study area.

396   The confluence of the underground river system plays an important role for the

397 confluence at the basin outlet. To facilitate the calculation of confluence in the QMG model,

398 the underground river systems can be generalized into large multiple conduit systems.

399 During floods, these conduit systems are mostly under pressure. Whether the water flow is

400 laminar or turbulent depends on the flow regime at that time. The water flow into these

401 conduits is calculated by the Hagen–Poiseuille equation and the Darcy–Weisbach equation

402 (Shoemaker et al., 2008):

403
$$\begin{cases} Q_{\text{laminar}} = -A\dfrac{gd^2\partial h}{32v\partial x} = -A\dfrac{\rho gd^2\Delta h}{32\mu\tau\Delta l} \\[4mm] Q_{\text{turbulent}} = -2A\sqrt{\dfrac{2gd\,|\Delta h|}{\Delta l\tau}}\log\left(\dfrac{H_c}{3.71d} + \dfrac{2.51v}{d\sqrt{\dfrac{2gd^3\,|\Delta h|}{\Delta l\tau}}}\right)\dfrac{\Delta h}{|\Delta h|} \end{cases} \tag{15}$$

404 Here, Q_{laminar} [L/s] is the water flow of the laminar flow in the conduit systems, A [dm^2] is

405 the conduit cross-sectional area, d [dm] is the conduit diameter, ρ [kg/dm^3] is the density

406 of the underground river, $v=\mu/\rho$ is the coefficient of kinematic viscosity, $\Delta h/\tau\Delta l$ is

407 the hydraulic slope of the conduits, τ is the dimensionless conduit curvature, $Q_{\text{turbulent}}$ [L/s]

408 is the turbulent flow in the conduit systems and H_c [dm] is the average conduit wall height.

409 **3.2 Parameter optimization**

410 In total, the QMG model has 12 parameters, of which flow direction and slope are

411 topographic parameters that can be determined from the DEM without parametric

412 optimization, while the remaining 10 parameters require calibration. Other distributed

413 hydrological models with multiple structures usually have many parameters. For example,

414 the Karst–Liuxihe model (Li et al., 2021) has 15 parameters that must be calibrated. In the

415 QMG model, each parameter is normalized as

416
$$x_i = x^*_i / x_{i0}, \tag{16}$$

417 where x_i is the dimensionless parameter value i after it is normalized, x^*_i is the parameter

418 value i in actual physical units, and x_{i0} is the initial or final value of x_i. Through the

419   processing of Eq. (16), the value range of the model parameters is limited to a hypercube

420   $K_n = (X \mid 0 \le x_i \le 1, \ i = 1, 2, ..., n)$, K is a dimensionless value. This normalized treatment

421   ignores the influence of the spatiotemporal variation of the underlying surface attributes on

422   the parameters, while also simplifying the classification and number of the model parameters

423   to a certain extent. Accordingly, the model parameters can be divided further into

424   rainfall-evaporation ones, epikarst-zone ones and underground-river ones. Table 1 lists the

425   parameters of the QMG model.

426   **Table 1.** Parameters of QMG model.

427   Because the QMG model has relatively few parameters, it is possible to calibrate them

428   manually, which has the advantage that the operation is easy to implement and does not

429   require a special program for parameter optimization. However, the disadvantage is that it is

430   subjective, which can lead to great uncertainty in the manual parameter calibration process.

431   To compare the effects of parameter optimization on model performance, this study used

432   both manual parameter calibration and the improved chaotic particle swarm optimization

433   algorithm (IPSO) for the automatic calibration of model parameters, and compared the

434   effects of both on flood simulation.

435   In general, the structure and parameters of a standard particle swarm optimization

436   algorithm (PSO) are simple, with the initial parameter values obtained at random. For

437   parameter optimization in high-dimensional multi-peak hydrological models, the standard

438   PSO is easily limited to a local convergence and cannot achieve the optimal effect, while the

439   late evolution of the algorithm may also cause problems, such as precocity and stagnant

440   evolution, due to the 'inert' aggregation of particles, which seriously affects the efficiency of

441   parameter selection. It is necessary to overcome the above problems and make the algorithm

442   converge to the global optimal solution with a high probability. In parameter optimization

443   for the QMG model, we improved the standard PSO algorithm by adding chaos theory, and

444   developed the IPSO, where 10 cycles of chaotic disturbances were added to improve the

445   activity of the particles. The inverse mapping equation of the chaotic variable is

446
$$\begin{cases} X_{ij} = X_{\min} + (X_{\max} - X_{\min}) * Z_{ij} \\ Z_{ij}^{'} = (1-\alpha)Z^{*} + \alpha Z_{ij} \end{cases} \tag{17}$$

447 where X_{ij} is the optimization variable for the model parameters, $(X_{max} - X_{min})$ is the

448 difference between its maximum and its minimum, Z_{ij} is the variable before the disturbance is

449 added and $Z_{ij}^{'}$ represents the chaotic variables after a disturbance is added, α is a variable

450 determined by the adaptive algorithm, $0 \leq \alpha \leq 1$, and Z^{*} is the chaotic variable formed when

451 the optimal particle maps to the interval [0,1]. In parameter optimization, the flowchart of the

452 IPSO is shown in Figure. 4.

453 **Figure 4.** Algorithm flow chart of IPSO.

454 **3.3 Uncertainty analysis**

455 Uncertainties in hydrological model simulation results usually originate from three aspects:

456 input data, model structure and model parameters (Krzysztofowicz, 2014). In the present

457 study, the input data (e.g. rainfall, flood events and some hydrogeological data) were first

458 validated and pre-processed through observations to reduce their uncertainties.

459 Second, we simplified the structure of the QMG model to reduce the structural

460 uncertainty. As a mathematical and physical model, a hydrological model has some

461 uncertainty in flood simulation and forecasting because of the errors in system structure and

462 the algorithm (Krzysztofowicz and Kelly, 2000). The model was designed with full

463 consideration of the relationship between the amount of data required to build the model and

464 its performance for flood simulation and forecasting in karst regions, and the model's entire

465 framework was integrated through simple structures and easy-to-implement algorithms,

466 using the concept of distributed hydrological modelling. Conventionally, the extent of

467 uncertainty is increased with the growing complexity of the model structure. We therefore

468 ensured that the structure of the QMG model was simple when it was designed, and the

469 model was divided into surface and underground double-layer structures to reduce its

470 structural uncertainty.

471 Third, we focus on analysing the uncertainty and sensitivity of the model parameters

472 and their optimization method, for which a multi-parametric sensitivity analysis method

473   (Choi et al., 1999; Li et al., 2020) was used to analyse the sensitivity of the parameters in the

474   QMG model. The steps in the parameter sensitivity analysis are as follows.

475   1) Selection of appropriate objective function

476   The Nash–Sutcliffe coefficient is widely used as the objective function to evaluate the

477   performance of hydrological models (Li et al., 2020, 2021). It was therefore used to assess

478   the QMG model. Because the most important factor in flood forecasting is the peak

479   discharge, it is used in the Nash coefficient equation:

480
$$NSC = 1 - \frac{\sum_{i=1}^{n}\left(Q_i - Q_i^{'}\right)^2}{\sum_{i=1}^{n}\left(Q_i - \overline{Q}\right)^2},$$
(18)

481   where NSC is the Nash–Sutcliffe coefficient, Q_i [L/s] are the observed flow discharges, Q_i'

482   [L/s] are the simulated discharges, $\overline{Q}$ [L/s] is the average observed discharge and n [h] is

483   the observation period.

484   2) Parameter sequence sampling

485   The Monte Carlo sampling method was used to sample 8000 groups of parameter

486   sequences. The parametric sensitivity of the QMG model was analysed and evaluated by

487   comparing the differences between the a priori and a posteriori distributions of the

488   parameters.

489   3) Parameter sensitivity assessment

490   The a priori distribution of a model parameter means its probability distribution, while

491   the a posteriori distribution refers to the conditional distribution calculated after sample

492   sampling, and it can be calculated based on the simulation result of the parametric

493   optimization. If there is a significant difference between the priori distribution and its

494   posteriori distributionthemof the parameter, then the parameter being tested has a high

495   sensitivity, whereas if there is no obvious difference, then the parameter is insensitive. The

496   parametric priori distribution is calculated as

$$\begin{cases} P_{i,j}(NSC_{i,j} \geq 0.85) = \dfrac{n}{N+1} \times 100 \\ \sigma_i = \sum_{j=1}^{n} \left(P_{i,j} - \overline{P_{i,j}} \right)^2 \end{cases} \qquad (19)$$

where $P_{i,j}$ is the a priori distribution's probability when $NSC_{i,j} \geq 0.85$. We used a simulated Nash coefficient of 0.85 as the threshold value, and n was the number of occurrences of a Nash coefficient greater than 0.85 in flood simulations. In each simulation, only a certain parameter was changed, while the remaining parameters remained unchanged. If the Nash coefficient of this simulation exceeded 0.85, then the flood simulation results were considered acceptable. The term σ_i is the difference between the acceptable value and its mean, which represents the parametric sensitivity ($0 < \sigma_i < 1$). The higher the σ_i value, the more sensitive the parameter. N is the 8000 parameter sequences, and $\overline{P_{i,j}}$ is the average value of the a priori distribution.

3.4 Model Setting

Once the model was built, some of the initial conditions had to be set before running it to simulate and forecast floods, such as basin division, the setting of initial soil moisture, and the assumption of the initial parameter range. 1) In the study area, the entire Qingmuguan karst basin was divided into 893 KHRUs, including 65 surface river units, 466 hill slope units, and 362 underground river units. The division of these units formed the basis for calculating the process of runoff generation and convergence. 2) The initial soil moisture was set to 0–100% of the saturation moisture content in the basin, and the specific soil moisture before each flood had to be determined by a trial calculation. 3) The waterhead boundary conditions of the groundwater were determined by a tracer test in the basin, where a perennial stable water level adjacent the groundwater-divide was used as the fixed waterhead boundary. The base flow of the underground river was determined to be 35 L/s from the perennial average dry season runoff. 4) The range of initial parameters and convergence conditions were assumed before parameter optimization (Figure 4). 5) Parameter optimization and flood simulation validated the performance of the QMG model

522 in karst basins.

4 Results and discussion

4.1 Parameter Sensitivity Results

525   The number of parameters in a distributed hydrological model is generally large, and it

526 is important to perform a sensitivity analysis of each parameter to quantitatively assess the

527 impact of the different parameters on model performance. In the QMG model, each

528 parameter was divided into four categories according to its sensitivity: (i) highly sensitive,

529 (ii) sensitive, (iii) moderately sensitive, and (v) insensitive. In the calibration of model

530 parameters, insensitive ones do not need to be calibrated, which can greatly reduce the

531 amount of calculation and improve the efficiency of model operation.

532   The flow process in the calibration period (14 April to 10 May 2017) was adopted to

533 calculate the sensitivity of the model parameters, for which the calculation principle was

534 equation (19), and the parameter sensitivity results are calculated in Table 2.

535   Table 2 Parametric sensitivity results in QMG model.

536   In Table 2, the value of σ_i [equation (19)] represents a parameter's sensitivity, and the

537 higher the value, the more sensitive the parameter is. From the results in Table 2, it was

538 found that the rainfall infiltration coefficient, rock permeability coefficient, rock porosity,

539 and the related parameters of soil water content, such as the saturated water content, and

540 field capacity, were sensitive parameters. The order of parameter sensitivity was as follows:

541 infiltration coefficient > permeability coefficient > rock porosity > specific yield > saturated

542 water content > field capacity > flow direction > thickness > slope > Soil coefficient >

543 channel roughness > evaporation coefficient.

544   In the QMG model, parameters are classified as highly sensitive, sensitive, moderately

545 sensitive, and insensitive according to their influence on the flood simulation results. In

546 Table 4, we divided the sensitivity of model parameters into four levels based on the σ_i

547 value: 1) highly sensitive parameters, $0.8 < \sigma_i < 1$; 2) sensitive parameters, $0.65 < \sigma_i < 0.8$;

548   3) moderately sensitive parameters, $0.45 < \sigma_i < 0.65$; and 4) insensitive parameters,

549    $0 < \sigma_i < 0.45$. The highly sensitive parameters were the infiltration coefficient, permeability

550   coefficient, rock porosity, and specific yield. The sensitive parameters were the saturated

551   water content, field capacity, and thickness of the epikarst zone. The moderately sensitive

552   parameters were flow direction, slope, and soil coefficient. The insensitive parameters were

553   channel roughness and the evaporation coefficient.

554   **4.2 Parametric Optimization**

555   In total, the QMG model has 12 parameters, of which only eight need to be optimized,

556   which is relatively few for distributed models. The parameters of flow direction and slope as

557   well as the insensitive parameters of channel roughness and the evaporation coefficient need

558   not be calibrated, which can improve the convergence efficiency of the model parameter

559   optimization.

560   In the study area, 18 karst floods during the period of 14 April 2017 to 10 June 2019

561   were recorded at the underground river outlet to validate the effects of the QMG model in

562   karst hydrological simulations. The calibration period was 14 April to 10 May 2017 at the

563   beginning of the flow process, with the remainder of the time being the validation period. In

564   the QMG model, the IPSO algorithm was used to optimize the model parameters. To show

565   the necessity of parameter optimization for the distributed hydrological model, the study

566   specifically compared the flood simulations obtained using the initial parameters of the

567   model (without parameter calibration) and the optimized parameters. Figure. 5 shows the

568   iteration process of parameter optimization for the QMG model.

569   Figure 5 Iteration process of parametric optimization.

570   Figure. 5 shows that almost all parameters fluctuated widely at the beginning of the

571   optimization, and then after about 15 iterations of the optimization calculation, most of the

572   linear fluctuations become significantly less volatile, which indicated that the algorithm

573   tended to converge (possibly only locally). When the number of iterations exceeded 25, all

574   parameters remained essentially unchanged, meaning that the algorithm had converged (at

575   this point there was global convergence). It took only 25 iterations to reach a definite

576 convergence of the parameter rates with this IPSO algorithm, which is extremely efficient in

577 terms of the parameter optimization of distributed hydrological models. In previous studies

578 of the parametric optimization for the Karst-Liuxihe model in similar basin areas, 50

579 automatic parameter optimization iterations were required to reach convergence (Li et al.,

580 2021), demonstrating the effectiveness of the IPSO algorithm.

581 To evaluate the effect of parameter optimization, the convergence efficiency of the

582 algorithm, and more importantly, the parameters after calibration were used to simulate

583 floods. Figure. 6 shows the flood simulation effects.

584 Figure 6 Flow simulation results of QMG model based on parameter optimization.

585 Figure. 6 shows that the flows simulated by parameter optimization were better than

586 those simulated by the initial model parameters. The simulated flow processes based on the

587 initial parameters were relatively small, with the simulated peak flows in particular being

588 smaller than the observed values, and there were large errors between the two values. In

589 contrast, the simulated flows produced by the QMG model after parameter optimization

590 were very similar to the observed values, which indicates that calibration of the model

591 parameters is necessary and that there was an improvement in parameter optimization

592 through the use of the IPSO algorithm in this study. In addition, it was found that the flow

593 simulation effect was better in the calibration periods than in the validation periods (Fig. 6).

594 To compare the results of the flow processes simulation with the initial model

595 parameters and the optimized parameters, six evaluation indices (Nash–Sutcliffe coefficient,

596 correlation coefficient, relative flow process error, flood peak error, water balance

597 coefficient, and peak time error) were applied in this study, and the results are presented in

598 Table 3.

599 Table 3 Flood simulation evaluation index through parametric optimization.

600 Table 3 shows that the evaluation indices of the flood simulations after parametric

601 optimization were better than those of the initial model parameters. The average values of

602 the initial parameters for these six indices 0.81, 0.74, 27%, 31%, 0.80, and 5 h, respectively.

603 For the optimized parameters, the average values were 0.90, 0.91, 16%, 14%, 0.94, and 3 h,

respectively. The flood simulation effects after parameter optimization clearly improved, implying that parameter optimization for the QMG model is necessary, and the IPSO algorithm for parameter optimization is an effective approach that can greatly improve the convergence efficiency of parameter optimization, and also ensure that the model performs well in flood simulations.

4.3 Model Validation in Flood Simulations

Following parameter optimization, we simulated the whole flow process (14 April 2017 to 10 June 2019) based on the optimized and initial parameters of the QMG model (Fig. 6), which enabled a visual reflection of the model used in the simulation of a long series of flow processes. To reflect the simulation effect of the model for different flood events, we divided the whole flow process into 18 flood events, then used the initial parameters of the model and the optimized parameters, respectively, to verify the model performance in flood simulations. Figure 7 and Table 4 show the flood simulation effects and their evaluation indices using both the initial and the optimized parameters.

Figure 7 Flood simulation effects based on initial and optimized parameters.

Table 4 Flood simulation indices for model validation.

Figure 7 shows that the flood simulation results using the initial parameters were smaller than the observed values, and the model performance improved in flood simulations after parameter optimization. The simulated flood processes were in good agreement with observations, and were especially effective for simulating flood peak flows. From flood simulation indices in Table 4, the average water balance coefficient based on the initial parameters was 0.69, i.e., much less than 1, indicating that the simulated water in the model was unbalanced. After parameter optimization, the average value was 0.92, indicating that parameter optimization had a significant impact on the model water balance calculation.

Table 4 shows that the average values of the six indices (Nash–Sutcliffe coefficient, correlation coefficient, relative flow process error, flood peak error, water balance coefficient, and peak time error) for the initial parameters were 0.79, 0.74, 26%, 25%, 0.69, and 5 h, respectively, while for the optimized parameters the average values were 0.92, 0.90,

632 10%, 11%, 0.92, and 2 h, respectively. All evaluation indices improved after parameter

633 optimization, with the average values of the Nash coefficient, correlation coefficient, and

634 water balance coefficient increasing by 0.13, 0.16, and 0.23, respectively. The average

635 values of the relative flow process error, flood peak error, and peak time error decreased by

636 15%, 14%, and 3 h, respectively. These reasonable flood simulation results confirmed that

637 parameter optimization by the IPSO algorithm was necessary and effective for the QMG

638 model.

639 Compared with the overall flow process simulation shown in Figure 6, each flood

640 process was better simulated by the QMG model (Fig. 7). This was because in the function

641 of the QMG model and its algorithm design, the main consideration was the calculation of

642 the flood process, but the correlation algorithm of the dry season runoff was not described

643 well enough. For example, equations (12)–(15) are the flood convergence algorithm. As a

644 result, the model is not good at simulating other flow processes, such as dry season runoff,

645 leading to a low accuracy in the overall flow process. The next phase of our research will

646 focus on refining the algorithm related to dry season runoff and improving the

647 comprehensive performance of the model.

648 **4.4 Uncertainty analysis**

649 **4.4.1 Assessment and reduction of uncertainty**

650 In general, the uncertainty in model simulation is due mainly to three aspects of the model:

651 (i) the uncertainty of its input data, (ii) the uncertainty of its structure and algorithm and (iii)

652 the uncertainty of its parameters. In the practical application of a hydrological model, these

653 three uncertainties are usually interwoven, which leads to the overall uncertainty of the final

654 simulation results (Krzysztofowicz, 2014). Therefore, the present study focused on the

655 uncertainties in the input data, the model structure and the parameters to reduce the overall

656 uncertainty of the simulation results.

657 First, the input data—mainly rainfall-runoff data and hydrogeological data—were

658 pre-processed, which substantially reduced their uncertainty. Second, we simplified the

659 structure of the QMG model, which is reflected in the fact that it has only two layers of

spatial structure in the horizontal and vertical directions. This relatively simple structure reduced greatly the uncertainty due to the model structure. In contrast, the underground structure of our previous Karst–Liuxihe model (Li et al., 2021) has five layers, which leads to great uncertainty. Third, appropriate algorithms for runoff generation and confluence were selected. Different models were designed for different purposes, which leads to great differences in the algorithms used. In the QMG model, most of the rainfall-runoff algorithms used have been validated by the research results of others, and some of them were improved to suit karst flood simulation and forecasting by the QMG model. For example, the algorithm for the generation of excess infiltration runoff [Eq. (2)] was an improvement of the version used in the Liuxihe model (Chen, 2009, 2018; Li et al., 2020). Finally, the algorithm for parameter optimization was improved. Considering the shortcomings of the standard PSO algorithm that tends to converge locally, this study developed the IPSO for parameter optimization by adding chaotic perturbation factors. The flood simulation results after parameter optimization were much better than those of the initial model parameters (Figs. 6 and 7 and Tables 2 and 3), which indicates that parameter optimization is necessary for a distributed hydrological model and can reduce the uncertainty of the model parameters.

4.4.2 Parameter sensitivity analysis

The parameter-sensitivity results in Table 2 show that the rainfall-infiltration coefficient in the QMG model was the most sensitive parameter. It was the key to determining the generation of excess infiltration surface runoff and separating surface runoff from subsurface runoff. If the rainfall infiltration coefficient was greater than the infiltration capacity, excess infiltration surface runoff was generated on the exposed karst landforms; otherwise, all rainfall would infiltrate to meet the water deficit in the vadose zone, and then continue to seep down into the underground river system, eventually flowing out of the basin through the underground river outlet. The confluence modes of surface runoff and underground runoff were completely different, resulting in a large difference in the simulated flow results. Therefore, the rainfall infiltration coefficient had the greatest impact on the final flood simulation results.

Other highly sensitive parameters such as the rock permeability coefficient, rock

porosity and specific yield were used as the basis for dividing between slow flow in karst fissures and rapid flow in conduits. The division of slow and rapid flows also had a great impact on the discharge at the outlet of the basin. Slow flow plays an important role in water storage in a karst aquifer and is very important for the replenishment of river base flow in the dry season. Rapid flow in large conduit systems dominates the flood runoff and is the main component of the flood water volume in the flood season.

Parameters related to the soil water content, including the saturated water content, field capacity and thickness, were sensitive parameters and had a large influence on the flood simulation results. This is because the soil moisture content prior to flooding affects how flood flows rise and when peaks occur. If the soil is already very wet or even saturated before the flooding, the flood will rise quickly to reach a peak, and the process line of the flood peak flow will be sharp and thin. This type of flood process forms easily and can lead to disaster-causing flood events. In contrast, if the soil in the basin is very dry before the flooding, the rainfall will first meet the water shortage of the vadose zone, and after it is replenished the rainfall will infiltrate into the underground river. The flood peak of the river basin outlet is therefore delayed.

The moderately sensitive parameters were flow direction, slope and the soil coefficient. They had a specific influence on the flood simulation results, but the influence was not as great as that of the highly sensitive and sensitive parameters. The insensitive parameters were channel roughness and the evaporation coefficient. The amount of water lost by evapotranspiration is very small in the total flood water, and it was therefore the least sensitive parameter in the QMG model.

5 Conclusions

This study proposed a new distributed physically based hydrological model, i.e. the QMG model, to simulate floods accurately in karst trough and valley landforms. The main conclusions of this paper are as follows.

This QMG model has a high application potential in karst hydrology simulations. Other distributed hydrological models usually have multiple structures, resulting in the need for a

large amount of data to build models in karst areas (Kraller et al., 2014). The QMG model has only a double-layer structure, with a clear physical meaning, and a small amount of basic data is needed to build the model in karst areas, such as some necessary hydrogeological data. For example, the distribution and flow direction of underground rivers is required, which can be inferred from a tracer test, leading to a low modelling cost. There were fewer parameters in the QMG model than in other distributed hydrological models, with only 10 parameters that needed to be calibrated.

The flood simulation after parameter optimization was much better than the simulation using the initial model parameters. After parameter optimization, the average values of the Nash coefficient, correlation coefficient and water balance coefficient increased by 0.13, 0.16 and 0.23, respectively, while the average relative flow process error, flood peak error and peak time error decreased by 15%, 14% and 3 h, respectively. Parameter optimization is necessary for a distributed hydrological model, and the improvement of the IPSO algorithm in this study was an effective way to achieve this.

In the QMG model, the rainfall infiltration coefficient I_c, rock permeability coefficient K, rock porosity R_p and the parameters related to the soil water content were sensitive parameters. The order of parameter sensitivity was infiltration coefficient > permeability coefficient > rock porosity > specific yield > saturated water content > field capacity > flow direction > thickness > slope > soil coefficient > channel roughness > evaporation coefficient.

This QMG model is suitable for karst trough and valley landform like this study areabasins, where the topography is conducive to the spread of flood water. Whether this model is applicable to other the karst areas of other landforms in non trough valley regions still needs to be verified in the future studies. In addition, the basin area is very small, where the hydrological similarity between different small basin areas varies greatly (Kong and Rui, 2003). The size of the area to be modelled has a great influence on the choice of model spatial resolution (Chen et al., 2017). Therefore, whether the QMG model is suitable for flood forecasting in large karst basins needs to be determined.

Model development.

This QMG model presented in this study uses the Visual Basic language programming. The general framework of the model and the algorithm consist of three parts: the modeling approach, the algorithm of rainfall-runoff generation and confluence, and the parameter optimization algorithm. As a free and open source hydrological modeling program (QMG model-V1.0), we provide all modeling packages, including model code, installation package, simulation data package and user manual, free of charge. It is important to note that the model we provide are for scientific research purposes only and should not be used for any commercial purposes. Creative Commons Attribution 4.0 International.

Model installation program can be downloaded from ZENODO, cite as JI LI. (2021, June 16). QMG model-V1.0. Zenodo. http://doi.org/10.5281/zenodo.4964701, and http://doi.org/10.5281/zenodo.4964697 (registration required). User manual can be downloaded from http://doi.org/10.5281/zenodo.4964754.

Code availability.

All code for the QMG model-V1.0 in this paper are available and free, the code can be downloaded from ZENODO, Cite as JI LI. (2021, June 16). QMG model-V1.0 code (Version v1.0). Zenodo. http://doi.org/10.5281/zenodo.4964709 (registration required).

Data availability.

All data used in this paper are available, findable, accessible, interoperable, and reusable. The simulation data and modelling data package can be downloaded from http://doi.org/10.5281/zenodo.4964727. The DEM was downloaded from the Shuttle Radar Topography Mission database at http://srtm.csi.cgiar.org. The land use-type data were downloaded from http://landcover.usgs.gov, and the soil-type data were downloaded from http://www.isric.org. These data were last accessed on 15 October 2020.

Author contributions. JIL was responsible for the calculations and writing of the whole

paper. DY helped conceive the structure of the model. ZF and JL provided significant

assistance in the English translation of the paper. MM provided flow data of the study area.

Competing interests.

The authors declare that they have no conflicts of interest.

Acknowledgments.

This study was supported by the National Natural Science Foundation of China (41830648),

the National Science Foundation for Young Scientists of China (42101031), Fundamental

Research Funds for the Central Universities (), Chongqing Natural Science Foundation

778 (cstc2021jcyj-msxm0007), the Chongqing Education Commission Science and technology

779 research Foundation (KJQN202100201), the drought monitoring, analysising and early

780 warning of typical prone-to-drought areas of Chongqing (20C00183), and the Open Project

781 Program of Guangxi Key Science and Technology Innovation Base on Karst Dynamics

782 (KDL & Guangxi 202009, KDL & Guangxi 202012).

References

Abbott, M. B., Bathurst, J. C., Cunge, J. A., O'Connell, P. E., and Rasmussen, J.: An Introduction to the European HydrologicSystem-System Hydrologue Europeen, 'SHE', a: History and Philosophy of a Physically-based, Distributed Modelling System,J. Hydrol., 87, 45–59, 1986a.

Abbott, M. B., Bathurst, J. C., Cunge, J. A., O'Connell, P. E., and Rasmussen, J.: An Introduction to the European Hydrologic System-System Hydrologue Europeen, 'SHE', b: Structure of a Physically based, distributed modeling System, J. Hydrol., 87,61–77, 1986b.

Ambroise, B., Beven, K., and Freer, J.: Toward a generalization of the TOPMODEL concepts: Topographic indices of hydrologic similarity. Water Resources Research, 32, 2135-2145, 1996.

Atkinson, T.C.: Diffuse flow and conduit flow in limestone terrain in the Mendip Hills, Somerset (Great Britain). Journal of Hydrology, 35, 93-110. https://doi.org/10.1016/0022-1694(77)90079-8, 1977.

Berry, R.A., Saurel, R., and Lemetayer, O.: The discrete equation method (DEM) for fully compressible, two-phase flows in ducts of spatially varying cross-section. Nuclear Engineering & Design, 240(11), 3797-3818, 2010.

Beven, K., and Binley, A.: The future of distributed models: Model calibration and uncertainty prediction. Hydrological Processes, 6, 279-298, 2006.

Birk, S., Geyer, T., Liedl, R., and Sauter, M.: Process-based interpretation of tracer tests in carbonate aquifers. Ground Water, 43(3), 381-388, 2005.

Bittner, D., Parente, M.T., Mattis, S., Wohlmuth, B., and Chiogna, G.: Identifying relevant hydrological and catchment properties in active subspaces: An inference study of a lumped karst aquifer model. ADVANCES IN WATER RESOURCES,135,550-560.

doi: 10.1016/j.advwatres.2019.103472, 2020.

Blansett, K. L., and Hamlett, J. M.: Challenges of Stormwater Modeling for Urbanized Karst Basins. Pittsburgh, Pennsylvania, an ASABE Meeting Presentation, Paper Number: 1009274. doi:10.13031/2013.29840, 2010.

Blansett, K. L.: Flow, water quality, and SWMM model analysis for five urban karst basins.. (Doctoral dissertation). The Pennsylvania State University,USA, 2011.

Bonacci, O., Ljubenkov, I., and Roje-Bonacci, T.: Karst flash floods: an example from the Dinaric karst Croatia. Nat. Hazards Earth Syst. Sci. 6, 195–203, 2006.

Chang, Y., and Liu, L.: A review of hydrological models in karst areas. Engineering investigation, 43,37-44, 2015.

Chen, G.M., Jia, J.Y., and Han, Q.: Research on inertia weight reduction strategy of Particle Swarm optimization algorithm. Journal of Xi'an Jiaotong University, 40(1),53-56, 2006.

Choi, J., Harvey, J. W., and Conklin, M. H.: Use of multi-parameter sensitivity analysis to determine relative importance of factors influencing natural attenuation of mining contaminants. the Toxic Substances Hydrology Program Meeting, Charleston,South Carolina, 1999.

Chen, Y. B.: Liuxihe Model, China Science and Technology Press, Beijing, China, 2009.

Chen, Y., Li, J., and Xu, H.: Improving flood forecasting capability of physically based distributed hydrological models by parameter optimization. Hydrol. Earth Syst. Sci. 20, 375-392. https://doi.org/10.5194/hess-20-375-2016, 2016.

Chen, Y., Li, J., Wang, H., Qin, J., and Dong, L.: Large watershed flood forecasting with high-resolution distributed hydrological model. Hydrol. Earth Syst. Sci. 21, 735-749. https://doi.org/10.5194/hess-21-735-2017, 2017.

Chen, Y.: Distributed Hydrological Models. Springer Berlin Heidelberg, Berlin, Germany. https://doi.org/10.1007/978-3-642-40457-3_23-1, 2018.

Dewandel, B., Lachassagne, P., Bakalowicz, M., Weng, P., and Malki, A.A.: Evaluation of aquifer thickness by analysing recession hydrographs. Application to the Oman

ophiolite hard-rock aquifer. Journal of Hydrology, 274,248-269, 2003.

Dubois, E., Doummar, J., Séverin Pistre, S., and Larocque, M.: Calibration of a lumped karst system model and application to the Qachqouch karst spring (Lebanon) under climate change conditions. Hydrol. Earth Syst. Sci., 24, 4275-4290. https://doi.org/10.5194/hess-24-4275-2020, 2020.

Doummar, J., Sauter, M., and Geyer, T.: Simulation of flow processes in a large scale karst system with an integrated catchment model (MIKE SHE) – identification of relevant parameters influencing spring discharge. Journal of Hydrology, 426-427, 112-123, 2012.

Epting, J., Page, R.M., and Auckenthaler, A.: Process-based monitoring and modeling of Karst springs–Linking intrinsic to specific vulnerability. Science of the Total Environment, 625, 403-415, 2018.

Fleury, P., Plagnes, V., and Bakalowicz, M.: Modelling of the functioning of karst aquifers with a reservoir model: Application to Fontaine de Vaucluse (South of France). Journal of Hydrology, 345,38-49. http://dx.doi.org/10.1016/j.jhydrol.2007.07.014, 2007b.

Ford, D. C., and Williams, P.W.: Karst geomorphology and hydrology. Wiley, Chichester, England, 2007.

Gang, L., Tong, F.G., and Bin,T.: A Finite Element Model for Simulating Surface Runoff and Unsaturated Seepage Flow in the Shallow Subsurface. Hydrological Processes, 6,102-120. doi: 10.1002/hyp.13564, 2019.

Geyer, T., Birk, S., Liedl, R., and Sauter, M.: Quantification of temporal distribution of recharge in karst systems from spring hydrographs. Journal of Hydrology, 348(30), 452-463, 2008.

Gou, P.F., Jiang, Y.J., Hu, Z.Y., Pu, J.B., and Yang, P.H.: A study of the variations in hydrology and hydrochemistry under the condition of a storm in a typical karst subterranean stream. HYDROGEOLOGY&ENGINEERING GEOLOGY,37(5),20-25, 2010.

862 Gutierrez, F.: Hazards associated with karst. In: Alcantara, I. & A. Goudie (Eds.),

863 Geomorphological Hazards and Disaster Prevention. Cambridge University Press,

864 Cambridge, 161–175, 2010.

865 Gutierrez, F., Parise, M., D'Waele, J., and Jourde, H.:   A review on natural and human-

866 induced geohazards and impacts in karst. Earth Science Reviews, 138, 61-88, 2014.

867 Hartmann, A., and Baker, A.: Progress in the hydrologic simulation of time variant of karst

868 systems-Exemplified at a karst spring in Southern Spain. Advances in Water Resources,

869 54,149-160, 2013.

870 Hartmann, A., Goldscheider, N., Wagener, T., Lange, J., and Weiler, M.: Karst water

871 resources in a changing world: Review of hydrological modeling approaches. Reviews

872 of Geophysics 52: 218-242. doi: 10.1002/2013RG000443, 2014a.

873 Hartmann, A., and Baker, A.: Modelling karst vadose zone hydrology and its relevance for

874 paleoclimate reconstruction. Earth-Science Reviews, 172, 178-192, 2017.

875 Hartmann, A.: Experiences in calibrating and evaluating lumped karst hydrological models.

876 London: Geological Society, Special Publications, 2018.

877 Jourde, H., Roesch, A., Guinot, V., and Bailly-Comte, V.: Dynamics and contribution of

878 karst groundwater to surface flow during Mediterranean flood. Environ. Geol. 51 (5),

879 725–730, 2007.

880 Jourde, H., Lafare, A., Mazzilli, N., Belaud, G., Neppel, L., Doerfliger, N., and Cernesson, F.:

881 Flash flood mitigation as a positive consequence of anthropogenic forcings on the

882 groundwater resource in a karst catchment. Environ. Earth Sci. 71, 573–583,2014.

883 Jukić, D., and Denić-Jukić, V.: Groundwater balance estimation in karst by using a

884 conceptual rainfall–runoff model. Journal of Hydrology, 373, 302-315.

885 http://dx.doi.org/10.1016/j.jhydrol.2009.04.035, 2009.

886 Kong, F.Z., and Rui, X.F.: Hydrological similarity of catchments based on topography.

887   GEOGRAPHICAL RESEARCH, (06), 709-715, 2003.

888   Kov ács, A., and Sauter, M.: Modelling karst hydrodynamics. In: Goldscheider N, Drew D

889   (eds) Methods in karst hydrogeology, IAH international contributions to hydrogeology;

890   26,264 p, 2007.

891   Kov ács, A., and Perrochet, P.: A quantitative approach to spring hydrograph decomposition.

892   Journal of Hydrology, 352, 16-29. http://dx.doi.org/10.1016/j.jhydrol.2007.12.009,

893   2008.

894   Kurtulus, B., and Razack, M.: Evaluation of the ability of an artificial neural network model

895   to simulate the input-output responses of a large karstic aquifer: the la rochefoucauld

896   aquifer (charente, france). Hydrogeology Journal, 15(2), 241-254, 2007.

897   Krzysztofowicz, R., and Kelly, K.: Hydrologic uncertainty processor for probabilistic river

898   stage forecasting. Water Resources Research, 36(11),3265-3277, 2000.

899   Krzysztofowicz, R.: Probabilistic flood forecast∶ Exact and approximate predictive

900   distributions. Journal of Hydrology, 517(1), 643-651, 2014.

901   Kraller, G., Warscher, M., Strasser, U., Kunstmann, H., and Franz, H.: Distributed

902   hydrological modeling and model adaption in high alpine karst at regional scale

903   (berchtesgaden alps, germany). Springer International Publishing Switzerland.

904   https://doi.org/10.1007/978-3-319-06139-9_8, 2014.

905   Ladouche, B., Marechal, J. C., and Dorfliger, N.: Semi-distributed lumped model of a karst

906   system under active management. Journal of Hydrology, 509,215-230, 2014.

907   Li, J., Chen, Y., Wang, H., Qin, J., Li, J., and Chiao, S.: Extending flood forecasting lead

908   time in a large basin by coupling WRF QPF with a distributed hydrological model,

909   Hydrol. Earth Syst. Sci. 21, 1279–1294. https://doi.org/10.5194/hess-21-1279-2017,

910   2017.

911   Li, J., Yuan, D., Liu, J., Jiang, Y., Chen, Y., Hsu, K. L., and Sorooshian, S.: Predicting floods

912   in a large karst river basin by coupling PERSIANN-CCS QPEs with a physically based

913   distributed hydrological model. Hydrol. Earth Syst. Sci. 23, 1505-1532.

https://doi.org/10.5194/hess-23-1505-2019, 2019.

Li, J., Hong, A., Yuan, D., Jiang,Y., Deng,S., Cao,C., and Liu, J.: A new distributed karst-tunnel hydrological model and tunnel hydrological effect simulations. Journal of Hydrology, 593, 125639. https://doi.org/10.1016/j.jhydrol.2020.125639, 2020.

Li, J., Hong, A., Yuan, D., Jiang,Y., Zhang,Y., Deng,S., Cao,C., Liu, J., and Chen,Y.: Elaborate Simulations and Forecasting of the Effects of Urbanization on Karst Flood Events Using the Improved Karst-Liuxihe Model.CATENA,197,104990. https://doi.org/10.1016/j.catena.2020.104990, 2021.

Liedl, R.., Sauter, M., Huckinghaus, D., Clemens, T., and Teutsch, G.: Simulation of the development of karst aquifers using a coupled continuum pipe flow model. Water Resources Research, 39, 50-57, 2003.

Liu, X., Jiang, Y.J., Ye, M.Y., Yang, P.H., Hu, Z.Y., and Li, Y.Q.: Study on hydrologic regime of underground river in typical karst valley- A case study on the Qingmuguan subterranean stream in Chongqing. CARSOLOGICA SINICA, 28(2),149-154, 2009.

Lu, D. B., Shi, Z. T., Gu, S. X., and Zeng, J. J.: Application of Hydrological Model in the Karst Area. Water-saving irrigation.11, 31-34. doi:1007-4929(2013)11-031-04, 2013.

Mario, T.P., Daniel, B., Steven, A. M., Gabriele, C., and Barbara, W.: Bayesian calibration and sensitivity analysis for a karst aquifer model using active subspaces. Water Resources Research, 55,342-356. doi: 10.1029/2019WR024739, 2019.

Martinotti, M.E., Pisano, L., Marchesini, I., Rossi, M., Peruccacci, S., Brunetti, M.T., Melillo, M.,Amoruso, G., Loiacono, P., Vennari, C., Vessia, G., Trabace, M., Parise, M., and Guzzetti, F.: Landslides, floods and sinkholes in a karst environment: the 1–6 September 2014 Gargano event, southern Italy. Natural Hazards and Earth System Sciences, 17, 467-480, 2017.

Meng, H.H., Wang, N.C., Su, W.C., and Huo, Y.: Modeling and application of karst semi-distributed hydrological model based on sinkholes. SCIENTIA GEOGRAPHICA SINICA, 5, 550-554. doi: 10.3969/j.issn.1000-0690.2009.04.014, 2009.

Meng, H.H., and Wang, N.C.: Advances in the study of hydrological models in karst basin. Progress in Geography, 29,1311-1318, 2010.

Pan, H.Y.: Hydrological model and application in karst watersheds. China University of Geosciences. Doctoral Dissertation, Wuhan, China, 2014.

Parise, M.: Hazards in karst, Proceedings Int. Conf. "Sustainability of the karst environment. Dinaric karst and other karst regions", IHP-Unesco, Series on Groundwater,2, 155-162, 2010.

Peterson, E.W., and Wicks, C. M.: Assessing the importance of conduit geometry and physical parameters in karst systems using the storm water management model (SWMM).Journal of Hydrology, 329, 1-2, 294-305, 2006.

Peterson, J.R., and Hamlett, J.M.: Hydrologic calibration of the SWAT model in a basin containing fragipan soils. JAWRA Journal of the American Water Resources Association. doi: 10.1111/j.1752-1688.1998. tb00952.x, 1998.

Petrie, R., Denvil, S., Ames, S.,et al.: Coordinating an operational data distribution network for CMIP6 data, Geosci. Model Dev., 14, 629–644,

https://doi.org/10.5194/gmd-14-629-2021, 2021.

Qin, J.G., and Jiang, Y.P.: A review of numerical simulation methods for CFP pipeline flow. Groundwater. 3, 98-100, 2014.

Reimann, T., Melissa, E., and Hill.: Modflow-cfp: a new conduit flow process for modflow–2005. Ground Water,47(3),321-325. doi:10.1111/j.1745-6584.2009.00561.x, 2009.

Ren, Q.W.: Water Quantity Evaluation Methodology Based on Modified SWAT Hydrological Modeling in Southwest Karst Area, China University of Geoscience, Wuhan, China, 2006.

Shoemaker, W.B., Cunningham, K.J., and Kuniansky, E.L.: Effects of turbulence on hydraulic heads and parameter sensitivities in preferential groundwater flow layers.

Water Resources Research, 44, 34-50. doi: 10.1029/2007WR006601, 2008.

Suo, L.T., Wan, J.W., and Lu, X.W.: Improvement and application of TOPMODEL in karst region. Carsologica Sinica, 26(1), 67-70, 2007.

Teixeiraparente, M., Bittner, D., Mattis, S.A., Chiogna, G , and Wohlmuth, B.: Bayesian calibration and sensitivity analysis for a karst aquifer model using active subspaces. Water Resources Research, 55, 342-356. doi: 10.1029/2019WR024739, 2019.

White, W.B.: Karst hydrology: recent developments and open questions. Eng. Geol. 65, 85–105, 2002.

Williams, P.W.: The role of the epikarst in karst and cave hydrogeology: a review. Int. J. Speleol. 37, 1–10, 2008.

Williams, P. W.: Book Review: Methods in Karst Hydrogeology, Nico Goldscheider and David Drew (eds). Hydrogeology Journal, 17,1025-1025, 2009.

Worthington, S., Ford, D., and Beddows, P.: Porosity and permeability enhancement in unconfined carbonate aquifers as a result of solution. Speleogenesis: evolution of karst aquifers, 2000.

Yang, P. H., Luo, J.Y., Peng, W., Xia, K.S., and Lin, Y.S.: Application of online technique in tracer test-A case in Qingmuguan subterranean river system, Chongqing, China. CARSOLOGICA SINICA, 27(3),215-220, 2008.

Yu, D., Yin, J., Wilby, R.L., Stuart, N. L., Jeroen, C., Lin, N., Liu, M., Yuan, H., Chen, J., Christel, P., Guan, M., Avinoam, B., Charlie, W. D., Tang, X., Yu, L., and Xu, S.: Disruption of emergency response to vulnerable populations during floods. Nature Sustainability, 3, 728–736. https://doi.org/10.1038/s41893-020-0516-7, 2020.

Yu, Q., Yang, P.H., Yu, Z.L., Chen, X.B., and Wu, H.: Dominant factors controlling hydrochemical variationg of karst underground river in different period, Qingmuguan,Chongqing. CARSOLOGICA SINICA, 35(2),134-143, 2016.

993   Zhang, Q.: Assesment on the intrinsic vulnerability of karst groundwater source in the

994   Qingmuguan karst valley. CARSOLOGICA SINICA, 31(1),67-73, 2012.

995   Zhu, C., and Li, Y.: Long-Term Hydrological Impacts of Land Use/Land Cover Change

996   From 1984 to 2010 in the Little River Basin, Tennessee. International Soil and Water

997   Conservation Research, 2(2), 11-21, 2014.

 Tables

999 Table 1 Parameters of the QMG model.

Parameters	Variable name	Physical property
Infiltration coefficient	I_c	Meteorology
Evaporation coefficient	λ	Vegetation cover
Soil thickness	h	Karst aquifer
Soil coefficient	S_b	Soil type
Saturated water content	S_c	Soil type
Rock porosity	R_p	Karst aquifer
Field capacity	F_c	Soil type
Permeability coefficient	K	Karst aquifer
Flow direction	F_d	Landform
Slope	S_0	Landform
Specific yield	S_y	Karst aquifer
Channel roughness	n	Landform

1000 Table 2 Parametric sensitivity results in QMG model.

I_c	λ	h	S_b	S_c	S_y	F_d	S_0	R_p	F_c	K	n
0.92	0.24	0.71	0.58	0.8	0.83	0.74	0.68	0.86	0.78	0.89	0.36

1001 Table 3 Flood simulation evaluation index through parametric optimization.

Parameter optimization	Parameter types	Nash coefficient	Correlation coefficient	Relative flow process error/%	Flood peak error/%	Water balance coefficient	Peak time error (hours)
calibration	initial	0.82	0.77	24	29	0.82	4
periods	optimized	0.91	0.94	14	12	0.95	2
validation	initial	0.79	0.71	29	32	0.77	6
periods	optimized	0.88	0.87	18	16	0.92	3
average	initial	0.81	0.74	27	31	0.8	5
value	optimized	0.9	0.91	16	14	0.94	3

1002 Table 4 Flood simulation indices for model validation.

Floods	Parameter types	Nash coefficient	Correlation coefficient	Relative flow process error/%	Flood peak error/%	Water balance coefficient	Peak time error/ (hours)
2017042408	initial	0.77	0.7	28	29	0.71	-5
	optimized	0.95	0.89	11	15	0.88	-2
2017050816	initial	0.78	0.71	19	19	0.76	-4
	optimized	0.92	0.88	11	9	0.94	-2
2017061518	initial	0.76	0.6	25	32	0.63	-5

	optimized	0.91	0.93	12	11	0.95	-3
2017071015	initial	0.78	0.82	25	37	0.64	-4
	optimized	0.92	0.87	8	7	0.94	-2
2017091512	initial	0.81	0.62	21	16	0.78	-5
	optimized	0.9	0.92	13	10	0.9	-4
2017100815	initial	0.75	0.68	30	26	0.62	-2
	optimized	0.94	0.86	11	15	0.92	-1
2018052016	initial	0.78	0.68	25	21	0.67	5
	optimized	0.91	0.93	10	13	0.94	2
2018060815	initial	0.82	0.79	27	22	0.69	-6
	optimized	0.9	0.92	11	12	0.93	-4
2018071212	initial	0.84	0.75	26	24	0.61	5
	optimized	0.91	0.88	8	15	0.92	3
2018081512	initial	0.71	0.78	26	24	0.78	-4
	optimized	0.89	0.94	12	11	0.89	-3
2018090516	initial	0.85	0.68	28	23	0.68	-5
	optimized	0.93	0.87	12	10	0.92	-2
2018092514	initial	0.79	0.78	23	19	0.59	5
	optimized	0.88	0.88	9	11	0.89	2
2018101208	initial	0.78	0.81	28	25	0.63	5
	optimized	0.92	0.94	11	10	0.94	2
2018111208	initial	0.79	0.81	25	24	0.65	-6
	optimized	0.94	0.86	13	12	0.92	-2
2019042512	initial	0.78	0.8	26	36	0.8	5
	optimized	0.89	0.94	9	16	0.93	2
2019051513	initial	0.84	0.77	32	27	0.79	4
	optimized	0.91	0.88	9	13	0.95	2
2019052516	initial	0.74	0.75	29	26	0.63	-5
	optimized	0.92	0.86	7	15	0.96	-2
2019060518	initial	0.85	0.83	28	25	0.78	-4
	optimized	0.95	0.96	10	12	0.92	-2
average value	initial	0.79	0.74	26	25	0.69	5
	optimized	0.92	0.9	10	11	0.92	2

1003 **Figures**
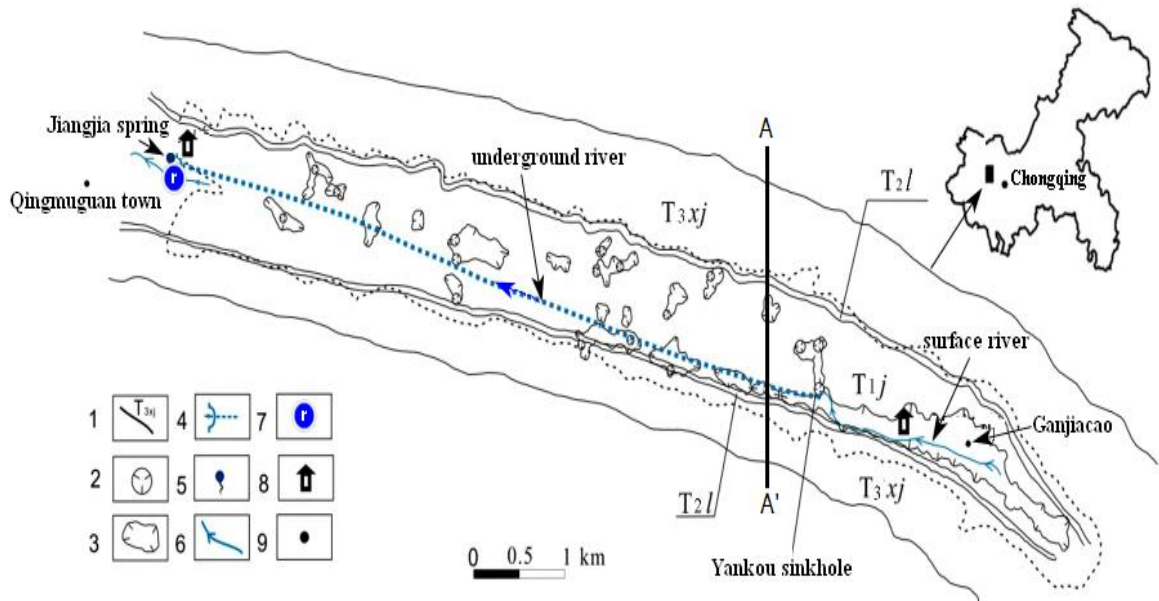
1004

1005   1- stratigraphic boundary, 2-sinkhole, 3- karst depression, 4- underground river, 5-
1006 karst spring, 6-surface river,7-river gauge, 8- rain gauge, and 9- geographical name
1007   a.   Qingmuguan karst basin (modified from Yu et al.,2016)
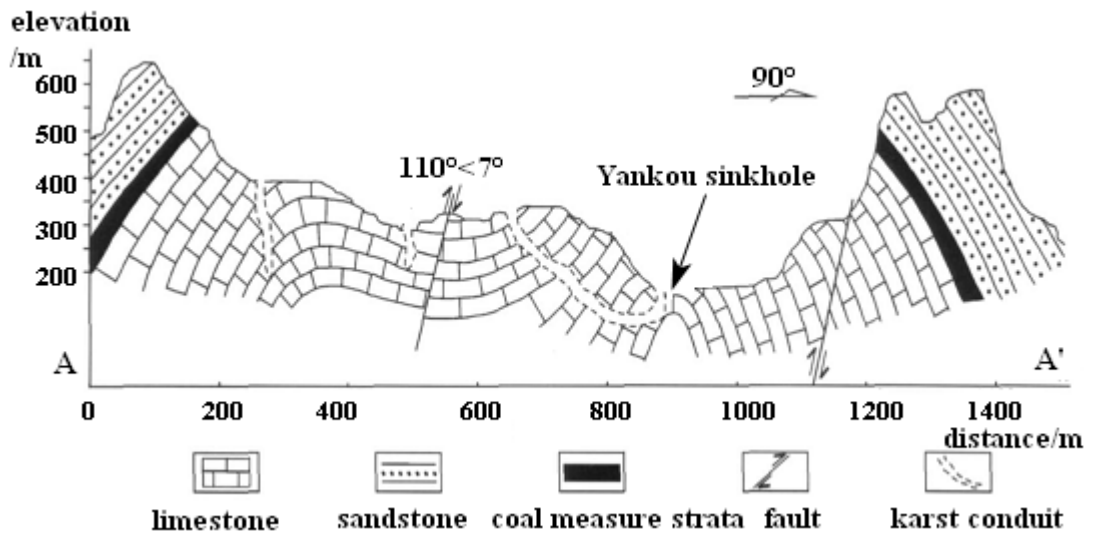
1008

1009   b. Lithologic cross section of Yankou sinkhole/AA'(modified from Zhang,2012)
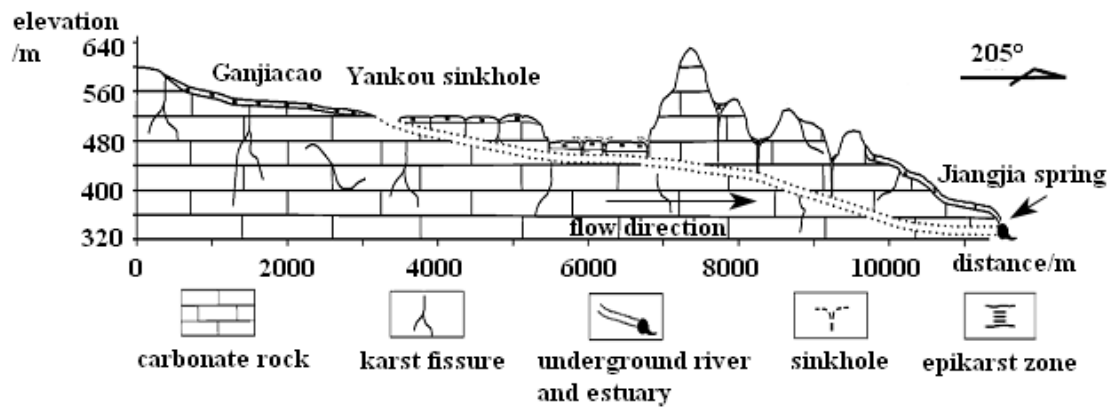
1010

1011   c. Longitudinal profile of the study area (modified from Yang et al.,2008)

1012   Figure 1 The Qingmuguan karst basin.

```
                        ┌─────────────┐
                        │ Model input │
                        └──────┬──────┘
       ┌───────────────────────┼──────────────────────┐
       ▼                       ▼                      ▼
┌──────────────┐   ┌──────────────────────┐   ┌─────────────┐
│ Rainfall and │   │ DEM, soil and land   │   │ Tracer test │
│ flow data    │   │ use data             │   └──────┬──────┘
└──────┬───────┘   └──────────┬───────────┘          ▼
                                            ┌──────────────────┐
                                            │ Hydrogeology data│
                                            └────────┬─────────┘
```

Surface runoff generation

Evapotranspiration, Interception and Spatial interpolation

Divide karst sub-basins

KHRUs division

Generalized karst aquifer

Flow direction and the distribution of river system

Surface runoff confluence calculation

DEM fill, slope and flow accumulation calculation

Structure improvement

Algorithm optimization

Rainfall infiltration

Underground runoff calculation

Uncertainty analysis

Parameter sensitivity analysis

Parameter optimization

Unsatisfactory

Flood simulation and forecasting

Model output

1013

1014   Figure 2 Modeling flow chart of QMG (Qingmuguan) model.
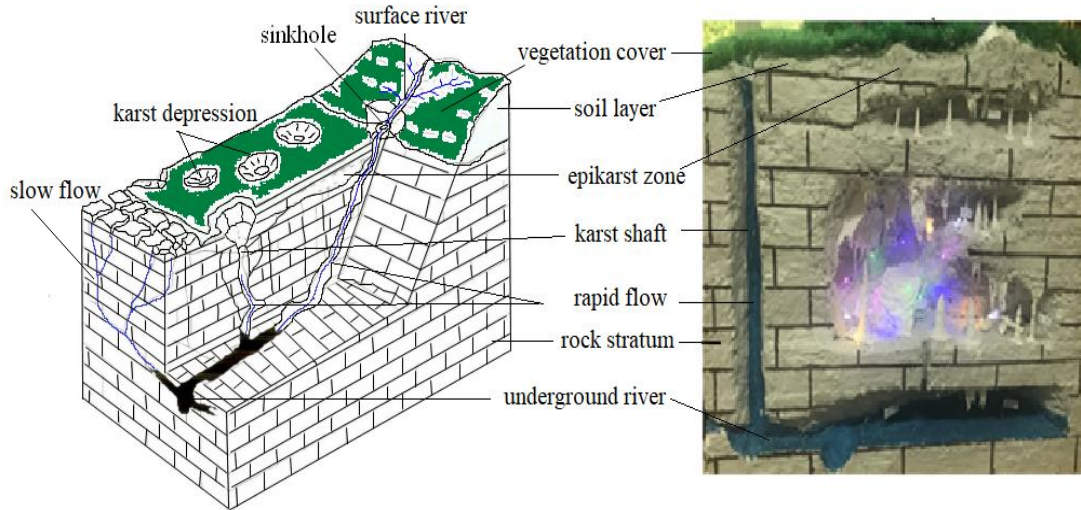
1015

1016   Figure 3 Spatial structure of the KHRUs (Li et al.,2021).
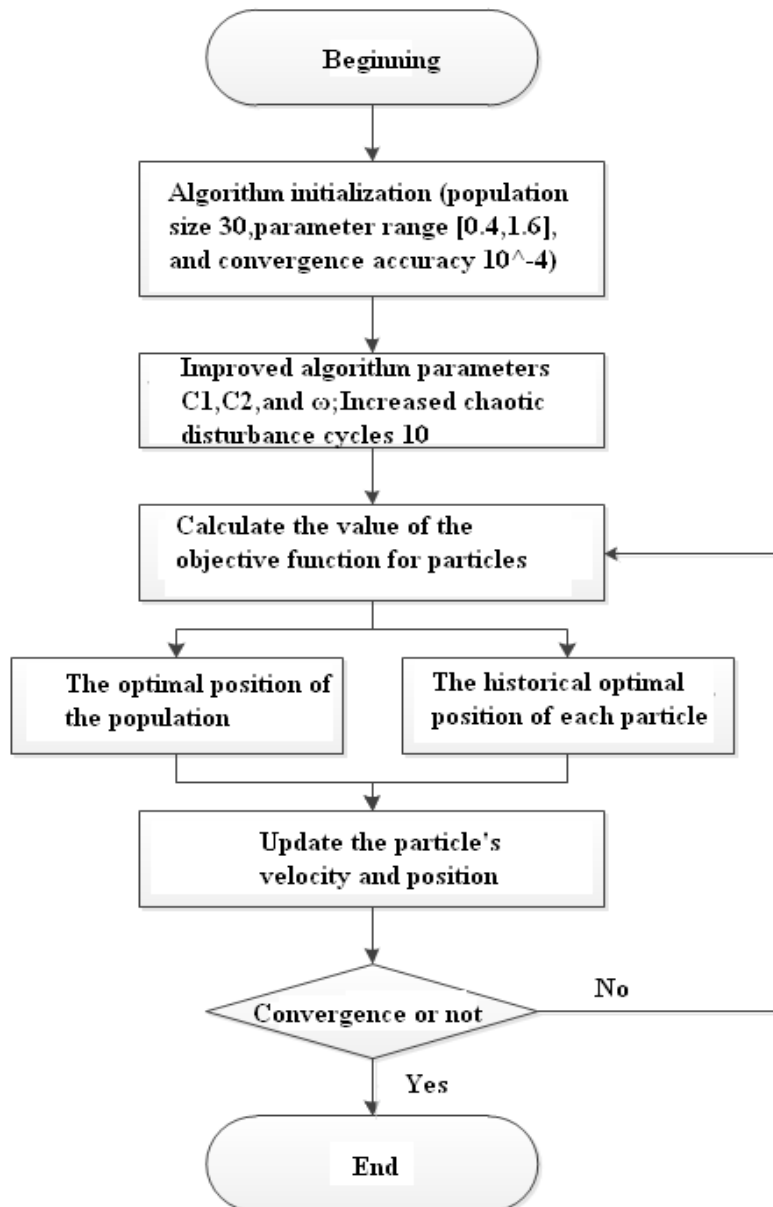
1017

1018   Figure 4 Algorithm flow chart of the IPSO.
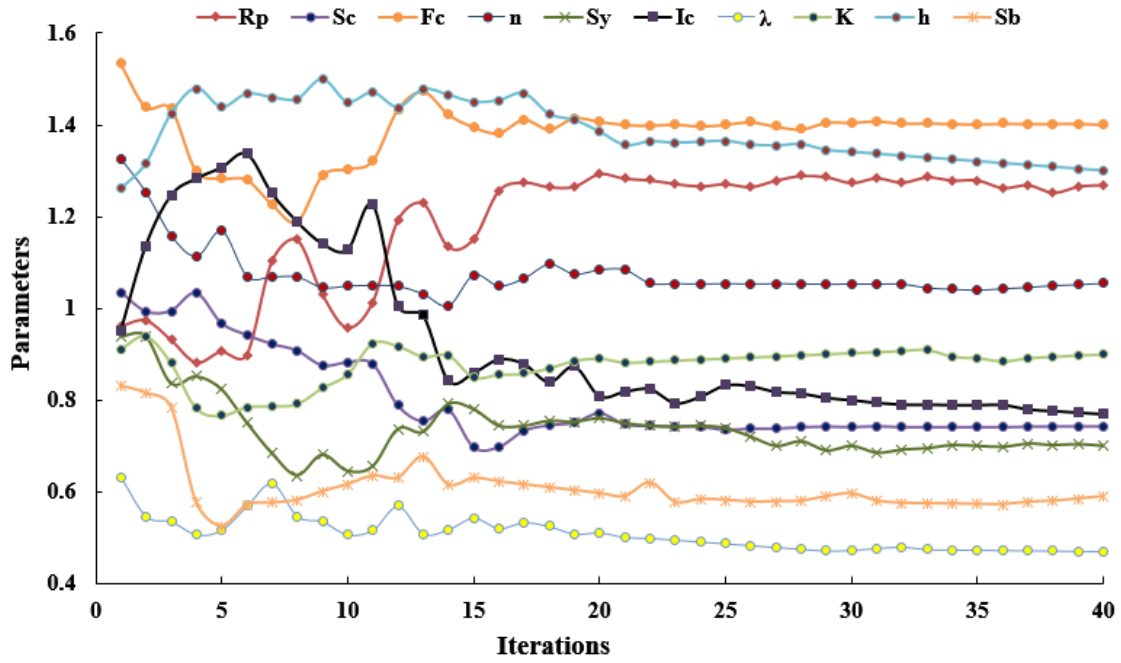
1019

1020   Figure 5 Iteration process of parametric optimization.
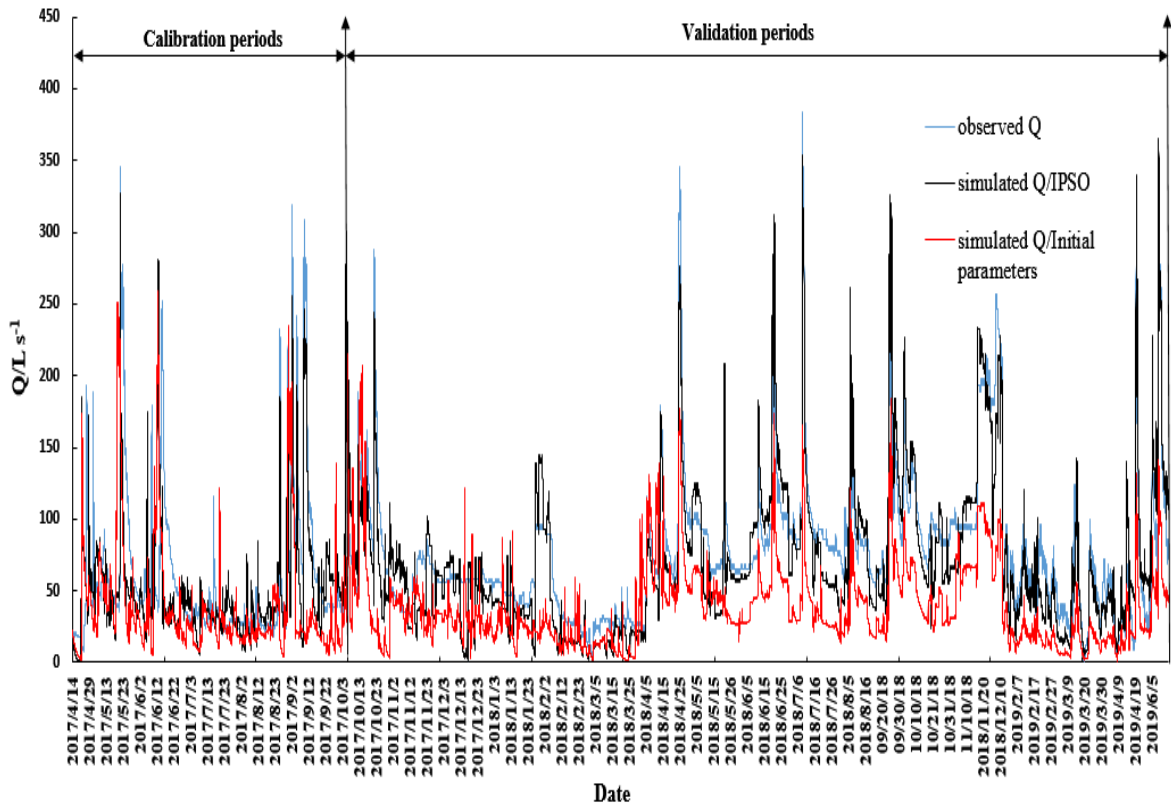
1021

1022   Figure 6 Flow simulation results of QMG model based on parameter optimization.
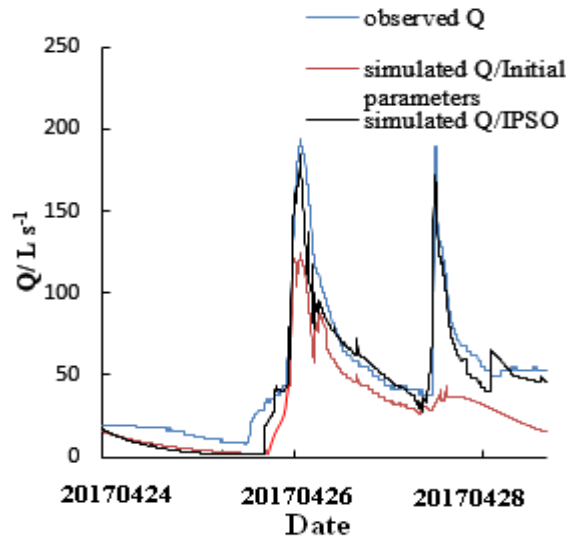
1023

1024   a. flood 201704240800   b. flood 201705081600
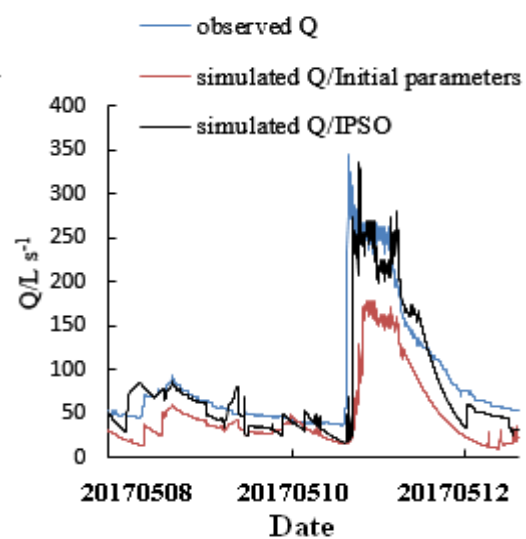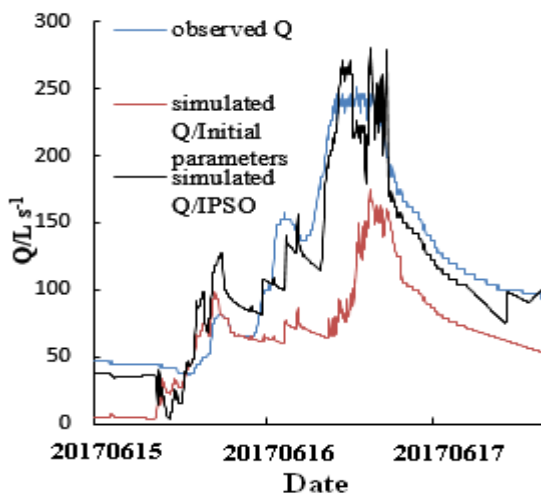
1025

1026   c.flood 201706151800   d. flood 201707101530
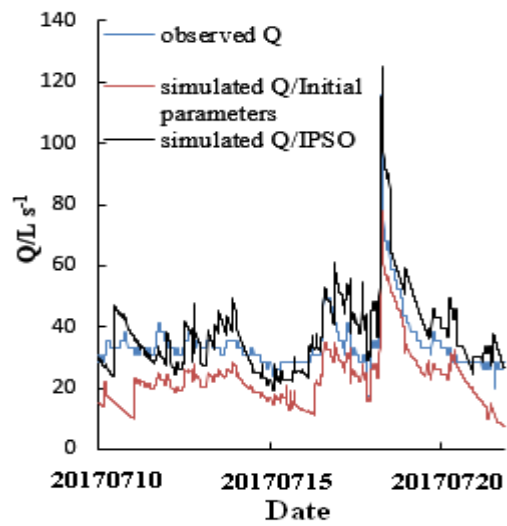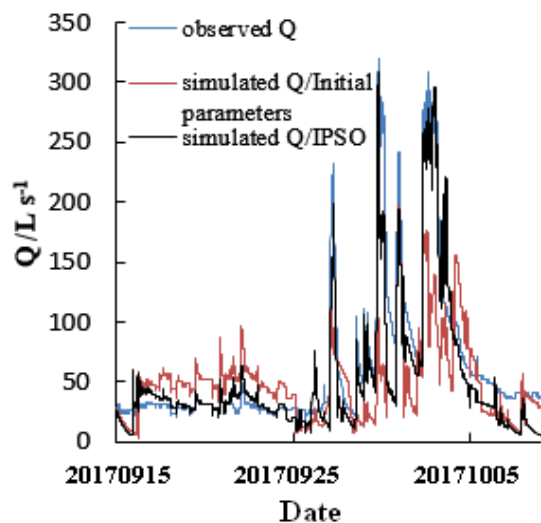
1027

1028   e.flood 201709151200   f.flood 201710081500
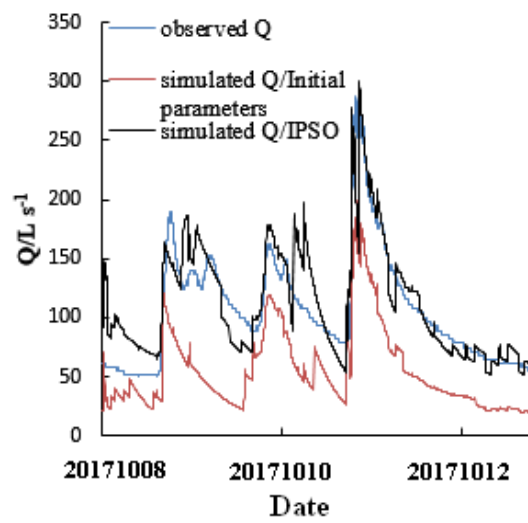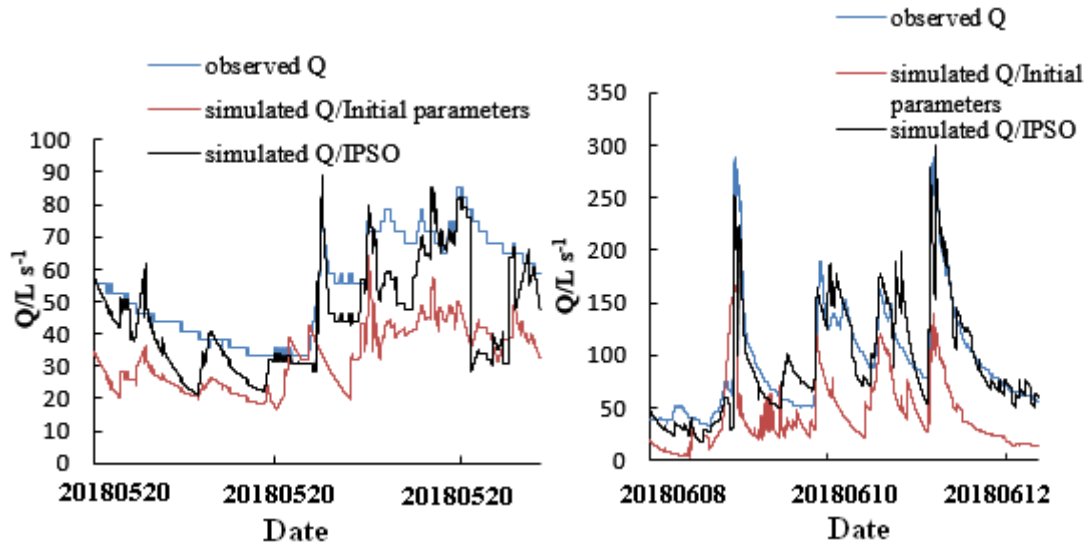
1029

1030   g.flood 201805201600   h.flood 201806081500
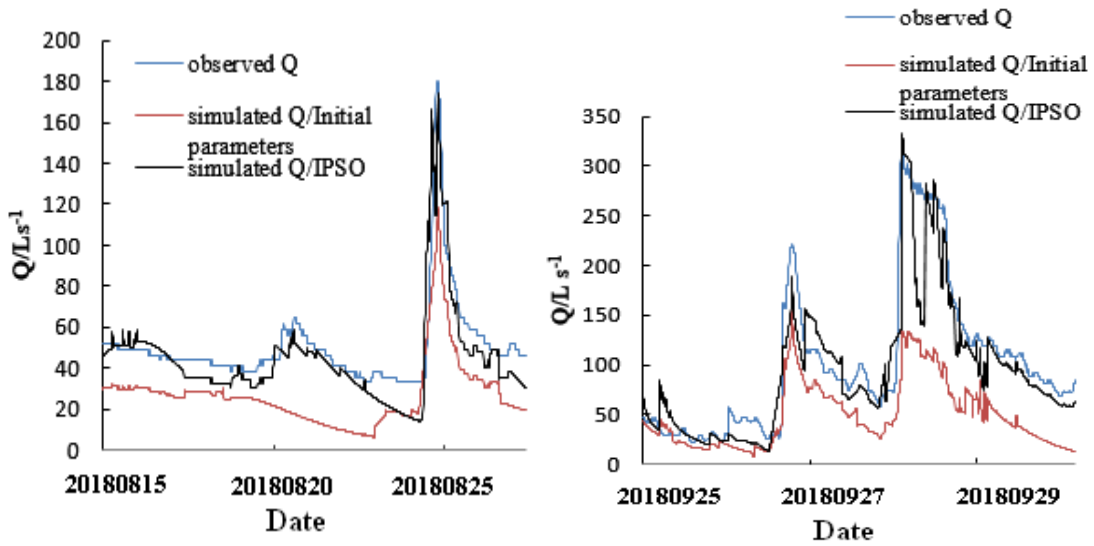
1031

1032   i.flood 201808151200   j.flood 201905251600

1033   Figure 7 Flood simulation effects based on initial and optimized parameters.